Low-energy bound states, resonances, and scattering of light ions

Benjamin K. Luna and T. Papenbrock

Phys. Rev. C **100**, 054307 — Published 6 November 2019

DOI: 10.1103/PhysRevC.100.054307

Low-energy bound states, resonances, and scattering of light ions

Benjamin K. Luna[1,2] and T. Papenbrock[3,4]

[1] *Department of Physics, Tennessee Technological University, Cookeville, Tennessee 38505, USA*
[2] *Joint Institute for Nuclear Physics and Applications, Oak Ridge National Laboratory, Oak Ridge, Tennessee 37831, USA*
[3] *Department of Physics and Astronomy, University of Tennessee, Knoxville, Tennessee 37996, USA*
[4] *Physics Division, Oak Ridge National Laboratory, Oak Ridge, Tennessee 37831, USA*

We describe bound states, resonances and elastic scattering of light ions using a δ-shell potential. Focusing on low-energy data such as energies of bound states and resonances, charge radii, asymptotic normalization coefficients, effective-range parameters, and phase shifts, we adjust the two parameters of the potential to some of these observables and make predictions for the nuclear systems $d+\alpha$, $^3\mathrm{H}+\alpha$, $^3\mathrm{He}+\alpha$, $\alpha+\alpha$, and $p+^{16}\mathrm{O}$. We identify relevant momentum scales for Coulomb halo nuclei and propose how to apply systematic corrections to the potentials. This allows us to quantify statistical and systematic uncertainties. We present a constructive criticism of Coulomb halo effective field theory and compute the unknown charge radius of $^{17}\mathrm{F}$.

I. INTRODUCTION

Low-energy reactions between light ions fuel stars and are relevant to stellar nucleosynthesis [1]. Because of the Coulomb barrier, fusion cross sections decrease exponentially with decreasing kinetic energy of the reactants, and this makes it difficult to measure them in laboratories. For the extrapolation of data to low energies, and a quantitative understanding of the reactions one thus has to turn to theoretical calculations.

Theoretical approaches can roughly be divided into two kinds, taking either the ions as degrees of freedom or starting from individual nucleons. The former approach includes a variety of models [2–5], effective range expansions [6–12], and effective field theories (EFTs) [13–18]; the microscopic approach ranges from simpler models [19] to ab initio computations [20–23]. Unfortunately, there are still significant uncertainties [1], and data tables for relevant quantities such as asymptotic normalization coefficients (ANCs) or astrophysical S factors may [24] or may not [25, 26] contain theoretical uncertainties.

There are various tools available for computing theoretical uncertainties [27, 28]. Systematic errors are accessible within EFTs (because of a power counting) [28–32] but much harder to quantify for models. Nevertheless, all models are constrained by data with errors, and the propagation of the latter to computed observables, or the employment of a set of models provides us with means to uncertainty estimates [27].

In this work, we revisit low-energy bound states, resonances, and scattering within simple two-parameter models, using ions as the relevant degrees of freedom. In an attempt to estimate uncertainties, we quantify the sensitivity of the computed results to the input data. We also propose systematic improvements of the simple models. This allows us to estimate model uncertainties. As we will see, this approach yields accurate results when compared to data. One of the key results is the prediction for the unknown charge radius of $^{17}\mathrm{F}$. We contrast our approach to Coulomb halo EFT (which is not accurate at leading order for $^8\mathrm{Be}$ [13] and $^{17}\mathrm{F}$ [14]) and present a constructive criticism based on a finite range and a modified derivative expansion.

This paper is organized as follows. In Section II we present arguments in support of finite-range interactions, review key formulas for the δ-shell potential, and discuss systematic improvements. Section III shows the results for a number of interesting light-ion systems. We conclude with a summary in Sect. IV. Several details are relegated to the Appendix V.

II. THEORETICAL BACKGROUND

A. Energy scales and estimates for observables

1. *Estimates for observables*

While effective range expansions [7–9, 33] established relations between low-energy observables, we still lack simple expressions that give estimates for such observables when only basic properties such as energies and radii of the involved ions are available. In applications of EFTs to low-energy ion scattering one makes assumptions about the relevant momentum scales to propose a power counting [13–15, 17]. This makes it important to understand the relevant scales. As it turns out, the presence of Coulomb interactions modifies expectations from neutron-halo EFT or pion-less EFT significantly. To see this, we explore how a finite-range potential differs from a zero-range potential.

The range of the strong nuclear force is close to the sum of the (charge) radii D of two interacting particles. This is true for both, the nucleon-nucleon interaction and for the strong force between ions considered in this work. It is in this sense that the nuclear interaction is short ranged. This implies that the two-body wave function essentially acquires its "free" asymptotic form for inter-particle distances $r \gtrsim D$.

The relevant asymptotic properties of a low-energy

bound-state wave function are its bound-state momentum (also known as the bound-state wave number) and ANC [34, 35]. In the absence of the Coulomb interaction, and for a zero-range interaction, the s-wave ANC C_0 is related to the bound-state momentum γ for weakly bound states via $C_0^2 \approx 2\gamma$. Similarly , the s-wave scattering length a_0 fulfills $a_0 \approx 1/\gamma$. This allows one – at leading order – to work with zero-range potentials whenever the physical range is sufficiently short and when the bound state momentum is the smallest momentum scale. We note that the effective range scales as $r_0 \sim \mathcal{O}(D)$. Finite-range effects of the potential enter at next-to-leading order. Pion-less EFT and neutron-halo EFT are based on these insights [36–38].

Let us now contrast this to the case when the Coulomb potential

$$V_C(r) = \frac{\hbar^2 k_c}{mr} \tag{1}$$

is added. Here, m is the reduced mass and k_c is the Coulomb momentum (or inverse Bohr radius)

$$k_c \equiv \frac{Z_1 Z_2 \alpha m}{\hbar}. \tag{2}$$

It is given in terms of the fine structure constant $\alpha \approx 1/137$ and the charge numbers Z_1 and Z_2 of the two ions. As we will see, this new momentum scale significantly modifies the discussion of low-energy observables.

We consider a weakly bound state with energy $-\hbar^2\gamma^2/(2m)$ and bound-state momentum γ, and assume $\gamma \ll k_c$; for resonances we consider a low-energy resonance with energy $\hbar^2\kappa^2/(2m)$ and momentum κ, and also assume $\kappa \ll k_c$. In what follows, we will simply refer to these momenta as k, setting $k = i\gamma$ for bound states and $k = \kappa$ for resonances. The Sommerfeld parameter is

$$\eta \equiv \frac{k_c}{k}. \tag{3}$$

For radial distances r approximately exceeding the sum D of the charge radii of the two ions, the strong interaction potential vanishes, and the Hamiltonian consists of the kinetic energy and the Coulomb potential. Thus, for $r \gtrsim D$, the wave functions are combinations of Coulomb wave functions. The key argument is as follows: For small momenta $|k| \ll k_c$, i.e. for $|\eta| \gg 1$, the Coulomb wave functions can be expanded in a series of modified Bessel functions, where coefficients fall off as inverse powers of η, while the modified Bessel functions have arguments $2\sqrt{2k_c r}$ (see the Appendix for details). Thus, low-energy observables (such as ANCs, radii, scattering lengths, and effective ranges) become series of functions of $2\sqrt{2k_c D}$, with coefficients that fall off as inverse powers of η. We have to distinguish the case of weak Coulomb $2\sqrt{2k_c D} \ll 1$ from the case of strong Coulomb (where $2\sqrt{2k_c D} \gg 1$). In the former case, one can take $D \to 0$ and employ zero-range interactions; in the latter case this is not possible. Estimates for several low-energy s-wave observables are given in Table I, and the results for $2\sqrt{2k_c D} \gg 1$ differ markedly from those where $D \to 0$ could be taken. The displayed results have been obtained with a δ-shell potential [8] (with details of the calculation presented in the Appendix).

Observable	$2\sqrt{2k_c D} \gg 1$	$D \to 0$
a_0	$-(\pi\kappa^2 D)^{-1} e^{4\sqrt{2k_c D}}$	$-\frac{6k_c}{\kappa^2}$
r_0	$(3k_c)^{-1}$	$\mathcal{O}(D)$
C_0	$(\pi D)^{-1/2}\Gamma(1+k_c/\gamma) e^{2\sqrt{2k_c D}}$	$\sqrt{6k_c}\Gamma(1+k_c/\gamma)$
$\frac{\Gamma}{E}$	$4\frac{k_c}{\kappa^2 D} e^{4\sqrt{2k_c D}} e^{-2\pi\frac{k_c}{\kappa}}$	$24\pi\frac{k_c^2}{\kappa^2} e^{-2\pi\frac{k_c}{\kappa}}$
$\langle r^2\rangle$	D^2	$\mathcal{O}(k_c^{-2})$

TABLE I. Simple estimates for low-energy observables of a two-ion system with a bound-state momentum γ or a resonance momentum κ, in presence of a Coulomb potential with the Coulomb momentum k_c, and a δ-shell potential with the range D, in the limit $\kappa, \gamma \ll k_c$. Here a_0, r_0, C_0, and Γ/E are the s-wave scattering length, effective range, and ANC, respectively. The resonance energy is $E = \hbar^2\kappa^2/(2m)$, and the corresponding width is denoted as Γ, not to be confused with the Gamma function $\Gamma(1+k_c/\gamma)$. The inter-ion distance is $\langle r^2\rangle$.

We see that the scattering length a_0, the squared ANC C_0^2, and the resonance width are exponentially enhanced by a factor $e^{4\sqrt{2k_c D}}$ when $k_c D \gg 1$ compared to the case $D \to 0$. We also see that the inter-ion distance squared $\langle r^2\rangle$ is not large, though we considered the limit of vanishing bound-state momentum. However, this distance becomes very small in the zero-range limit. It is clear that a zero-range potential is not compatible with nuclei that consist of ions: As ions have finite charge radii they must be separated by a distance that is similar to the sum of their charge radii in order to retain their identities. An EFT that employs a contact at leading order fails short of this requirement. These arguments confirm the need to include finite-range potentials or a finite effective range at leading order [13, 39, 40]. Bounds for the minimum physical range of the strong potential are also known from elementary considerations [41] and causality arguments [42, 43].

On the first view, the quantities displayed in the second column of Table I appear to be model dependent for $2\sqrt{2k_c D} \gg 1$ (as they depend on the parameter D). However, in the considered limit, the inter-ion distance fulfills $\langle r^2\rangle = D^2$, and this links observable quantities to each other.

The inter-ion distance is related to the charge radius. Let the ions (labeled by $i = 1, 2$) have masses m_i and charge radii squared $\langle r_i^2\rangle$. Then, the charge radius squared of the bound state is [44]

$$\langle R_c^2\rangle = \frac{Z_1\langle r_1^2\rangle + Z_2\langle r_2^2\rangle}{Z_1 + Z_2} + \frac{(Z_1 m_2^2 + Z_2 m_1^2)\langle r^2\rangle}{(Z_1 + Z_2)(m_1 + m_2)^2}. \tag{4}$$

Here, the first term account for the finite charge radii of the ions, and the second term is the contribution of the ions (taken as point charges) in the center-of-mass system. The derivation of Eq. (4) is elementary and this expression is well known [2, 44]; for a recent EFT dis-

cussion of contributions to charge radii in halo nuclei we refer the reader to Ref. [45]. We note that the consistency of any two-ion model (or EFT) requires that the distance between the two ions is larger than the sum of their individual charge radii. As we will see below, our results are largely consistent with the assumption of separated ions.

We also note that cluster systems consisting of an even-even and an odd-mass nucleus have magnetic moments (in units of nuclear magnetons)

$$\mu = \mu_{\rm odd} + \frac{Z}{A} l. \tag{5}$$

Here, $\mu_{\rm odd}$ is the magnetic moment of the odd-mass constituent, l is the orbital angular momentum, and Z and A are the charge and mass number, respectively, of the compound system. Here we assumed that the magnetic moment due to the spin S of the odd-mass ion and the magnetic moment due to the orbital angular momentum l add up. This is the case for states with total spin $j = l + S$. When applied to weakly bound nuclei, Eq. (5) serves as a check to what extend these nuclei can be viewed as clusters of two ions.

We note that (for $2\sqrt{2k_cD} \gg 1$) the effective range in Table I does not depend on D, and that it decreases with increasing Coulomb momentum. Its value, $r_0 = 1/(3k_c)$, is that of a Coulomb system with a zero-energy bound state (see Appendix for details), and $1/(3k_c)$ is also at the causality limit imposed by the Wigner bound [8, 43]. We can define the nontrivial regime of strong Coulomb interactions by the model-independent relation $3k_cr_0 \approx 1$. For the δ-shell potential, it is interesting to compute corrections that are due to a finite value of $2k_cD$. This yields [8] (see the Appendix for details)

$$r_0 - \frac{1}{3k_c} = -\pi D e^{-4\sqrt{2k_cD}}. \tag{6}$$

This equation expresses model-dependent quantities on its right-hand side in terms of observables. Combining it with the expression for the scattering length in Table I yields the model-independent relation

$$\kappa^{-2} = a_0 \left(r_0 - \frac{1}{3k_c} \right). \tag{7}$$

This formula was derived (for bound states) by Sparenberg *et al.* [9] and very recently rederived by Schmickler *et al.* [40].

Other notable relations that can be obtained from Table I are

$$a_0 \approx -(4\pi k_c)^{-1} \frac{\Gamma}{E} e^{2\pi \frac{k_c}{\kappa}}, \tag{8}$$

relating the scattering length to resonance properties, and

$$C_0^2 \approx \gamma^2 a_0 \left[\Gamma(1 + k_c/\gamma)\right]^2, \tag{9}$$

relating the ANC to the bound-state energy and the scattering length (after replacing κ by γ). This last expression agrees with the result in Refs. [9, 33, 43]. It seems to us that Eq. (8) was not yet known. These model-independent expressions are valuable. They relate quantities that are often unknown or hard to measure (such as the ANC or the effective range parameters) to others that are better known (such as energies or widths).

System	J^π	γ or κ (fm^{-1})	k_c (fm^{-1})	D (fm)	$2\sqrt{2k_cD}$
$d + \alpha$	1^+	0.31	0.09	3.82	1.68
^{3}H $+ \alpha$	$3/2^-$	0.45	0.12	3.43	1.80
^{3}He $+ \alpha$	$3/2^-$	0.36	0.24	3.64	2.63
$p + {}^7$Be	$1/2^-$	0.08	0.12	3.52	1.85
$\alpha + \alpha$	0^+	0.09	0.28	3.35	2.72
$p + {}^{16}$O	$1/2^+$	0.07	0.26	3.58	2.73

TABLE II. Bound-state momentum γ (or momentum κ of the resonant state), Coulomb momentum k_c, and sum of charge radii D for two-ion systems in the state with spin/parity J^π. The dimensionless quantity $2\sqrt{2k_cD}$ is also shown.

We believe the model-dependent expressions in Table I are also useful, because they allow us to estimate these hard-to-measure quantities. Table II lists relevant parameters for two-ion systems of interest. Of the considered systems, only the last two approximately fulfill both $|\eta| \gg 1$ and $2\sqrt{2k_cD} \gg 1$. Thus, for theses systems, finite-range models will yield significantly different values than zero-range models. Applying the simple expressions of Table I and the estimates for D from Table II to $\alpha - \alpha$ scattering, for instance, yields a very large scattering length of about $a_0 \approx -2482$ fm, an effective range $r_0 \approx 1.2$ fm, and a resonance width of $\Gamma \approx 7.5$ eV. These values are reasonably close to actual values. For the weakly bound $J^\pi = 1/2^+$ state of the $p + {}^{16}$O system, for example, we note that the simple estimate from Table I yields an ANC of about $C_0 \approx 80$ fm$^{-1/2}$, close to the empirical estimates [10, 26, 46, 47]. Thus, δ-shell potential allows us to estimate the sizes of relevant observables in Coulomb halo nuclei.

Table II shows that $2\sqrt{2k_cD} \gtrsim 1$ for essentially all Coulomb halo nuclei of interest. As a consequence, $r_0 - 1/(3k_c)$ is very small for s waves, and this makes scattering lengths, resonance widths, and ANCs large. We note that these are natural properties of Coulomb-halo nuclei. In contrast, the smallness of $r_0 - 1/(3k_c)$ is viewed as a fine tuning in Coulomb halo EFT [13, 14, 16].

Throughout this work, we will employ a single partial wave for the description of low-energy phenomena. Thus, we tacitly assume that the mixing of partial waves is a small correction that can be neglected at the precision we are working at. In this sense, the ANCs and resonance widths are single-particle properties.

2. *Energy scales*

In what follows, we will exploit a separation of scales between the low momentum scale we are interested in and a higher-lying breakdown scale. The breakdown momentum Λ_b defines the breakdown energy $E_b \equiv \hbar^2\Lambda_b^2/(2m)$.

It is set by the smaller of an empirical and a theoretical breakdown scale. The empirical breakdown scale is set by the energy of excited states of the two clusters or of the resulting nucleus; however, only states with relevant quantum numbers count. In ^{8}Be, for instance, the ground state has spin/parity $J^\pi = 0^+$, and the empirical breakdown scale is set by first excited 0^+ state at about 20 MeV (and not by the energy of the lowest 2^+ state at 3 MeV). There is also a theoretical breakdown scale. The strong interaction potential has a range that is of the size of the sum D of the charge radii of the clusters involved. Thus, at momenta π/D, the details of our model are fully resolved. As we cannot expect that the δ-shell model would be accurate at such a high momentum, π/D sets the theoretical breakdown momentum. In other words: when probed at this momentum scale, different models that exhibit the same physical range D will yield different results for obsevables.

The phenomena we seek to describe are simple because of a separation of scales. Scattering phase shifts at low energies are typically either close to zero or close to π. Only in presence of a narrow resonance do phase shifts vary rapidly in a small energy region of the size of the resonance width. Thus, away from the resonance energy, the asymptotic wave function consists mostly of the regular Coulomb wave function, which is exponentially small under the Coulomb barrier. This implies that the wave function cannot resolve any details of a finite-range potential as long as the classical turning point is larger than the range D of our potential, i.e. the strong potential is entirely in the classically forbidden region. The corresponding "model" momentum Λ_m fulfills

$$\Lambda_m \equiv \sqrt{2k_c/D}. \tag{10}$$

Thus, for energies below $E_m \equiv \hbar^2\Lambda_m^2/(2m)$, it will be hard to distinguish between different finite-range models that have been adjusted to low-energy data. In this sense, one deals with universal and model-independent phenomena. For momenta k with $\Lambda_m \lesssim k \lesssim \pi/D$ differences between models start to show up and eventually become fully resolved. Some models might accurately describe data even for momenta beyond Λ_m; we would view such models as fortuitous but useful picks. The systematic improvements that are presented in Subsection II C below can be used to estimate what a different model would yield; we refer to resulting uncertainties as "systematic uncertainties" in what follows. In EFT parlance, the momentum regime below Λ_m would be that where "leading-order" results are expected to be accurate and precise. Higher-order corrections should become visible beyond that scale.

In this work, we employ simple finite-range models for the nuclear potential that essentially exhibit two parameters (a range and a strength). Most calculations will be done with the δ-shell potential, but for ^{8}Be we also employ a simple square well or the Breit model [48], a hard-core potential plus a boundary condition. As we will see, at sufficiently low energies, and when adjusted to low-energy data, such simple models will describe data accurately and precisely. We will also propose how to make systematic improvements to these models.

B. δ-shell potential

The δ-shell potential plus the Coulomb interaction is well understood and can be solved analytically [7, 8, 49]. In this Subsection, we briefly summarize some of the relevant results. The Hamiltonian is

$$H = H_0 + V. \tag{11}$$

The strong interaction potential is V, and the "free" Hamiltonian H_0 consists of the kinetic energy and the Coulomb interaction

$$H_0 = -\frac{\hbar^2}{2m}\Delta + V_C(r). \tag{12}$$

Here, m denotes the reduced mass of the two-ion system and V_C is the Coulomb potential (1). The δ-shell potential is parameterized as

$$V(r) = \frac{\hbar^2\lambda_0}{2m}\delta(r-R). \tag{13}$$

Here, λ_0 and R denote the strength and the physical range of the potential, respectively. We work in the center-of-mass system and employ spherical coordinates. The radial wave function $\psi_l(r) = u_l(r)/r$ must be continuous at $r = R$, and its derivative $u_l' \equiv \frac{du_l}{dr}$ fulfills

$$u_l'(R^+) - u_l'(R^-) = \lambda_0 u_l(R). \tag{14}$$

The radii R^+ and R^- are infinitesimal larger and smaller than R, respectively.

As we shall see below, the δ-shell potential is quite useful in describing the low-energy physics of charged ions. The key is here that the outside ($r > R$) wave function has accurate asymptotic properties, and that low-energy physics does not probe the inaccurate and unphysical inside ($r < R$) wave function.

1. Bound states

For bound states with energy $E = -\frac{\hbar^2\gamma^2}{2m}$ we make the ansatz

$$u_l(r) = \begin{cases} N\frac{H_l^+\left(\frac{k_c}{i\gamma}, i\gamma R\right)}{F_l\left(\frac{k_c}{i\gamma}, i\gamma R\right)} F_l\left(\frac{k_c}{i\gamma}, i\gamma r\right), & r < R \\ N H_l^+\left(\frac{k_c}{i\gamma}, i\gamma r\right), & r > R. \end{cases} \tag{15}$$

Here, we employed the Coulomb wave functions F_l and H_l^+. We note that some readers might find the appearance of the Coulomb wave function H_l^+ unusual and might have preferred to see the Whittaker function $W_{-k_c/\gamma, l+1/2}(2\gamma R)$ instead. For complex arguments the

Coulomb wave function $H_l^+(-ik_c\gamma, i\gamma r)$ can be written in terms of the Whittaker function $W_{-k_c/\gamma,l+1/2}(2\gamma R)$, see Ref. [50, Chapter 33.2]. As we employ the Coulomb wave functions at imaginary arguments, some care must be taken in their numerical implementation; we followed Gaspard and Sparenberg [51] and present details in the Appendix. We also refer the reader to that reference for a discussion of the analytical properties (or lack thereof) of Coulomb wave functions. We recall that the Coulomb wave functions $F_0(\eta, x)$, $G_0(\eta, x)$, and $H_0^{\pm}(\eta, x)$ behave asymptotically, i.e. for large real values of the argument x and real values η, as the functions $\sin x$, $\cos x$, and $\exp(\pm ix)$ when omitting the Coulomb phase.

In Eq. (15), the constant N ensures the proper normalization

$$\int_0^\infty dr\,|u_l(r)|^2 = 1 \tag{16}$$

of the wave function. Because of the particular ansatz of the wave function for $r > R$ in terms of the Coulomb wave function rather than the Whittaker function, the ANC is

$$C_l = N\frac{W_{-k_c/\gamma,l+1/2}(2\gamma R)}{H_l^+\left(\frac{k_c}{i\gamma}, i\gamma R\right)}. \tag{17}$$

The matching condition (14) yields

$$\frac{\gamma}{\lambda_0} = iF_l\left(\frac{k_c}{i\gamma}, i\gamma R\right)H_l^+\left(\frac{k_c}{i\gamma}, i\gamma R\right). \tag{18}$$

The inter-ion distance squared

$$\langle r^2\rangle = \int_0^\infty dr r^2\,|u_l(r)|^2 \tag{19}$$

enters into the computation of the charge radius (4).

2. Scattering

For positive energies $E = \frac{\hbar^2k^2}{2m}$ we make the ansatz

$$u_l(r) = \begin{cases} BF_l\left(\frac{k_c}{k}, kr\right), & r < R \\ F_l\left(\frac{k_c}{k}, kr\right)\cos\delta + G_l\left(\frac{k_c}{k}, kr\right)\sin\delta, & r > R. \end{cases}$$

Here, G_l is the irregular Coulomb wave function, δ denotes the phase shift, and we employed the shorthand

$$B \equiv \frac{F_l\left(\frac{k_c}{k}, kR\right)\cos\delta + G_l\left(\frac{k_c}{k}, kR\right)\sin\delta}{F_l\left(\frac{k_c}{k}, kR\right)}. \tag{20}$$

The matching condition (14) yields

$$\frac{k}{\lambda_0} = -F_l^2\left(\frac{k_c}{k}, kR\right)\cot\delta - F_l\left(\frac{k_c}{k}, kR\right)G_l\left(\frac{k_c}{k}, kR\right) \tag{21}$$

Given the phase shifts, one can use this equation to adjust λ_0. Alternatively, for fixed parameters (λ_0, R) this equation can be solved for the phase shifts. This yields

$$\cot\delta = -\frac{\frac{k}{\lambda_0} + F_l\left(\frac{k_c}{k}, kR\right)G_l\left(\frac{k_c}{k}, kR\right)}{F_l^2\left(\frac{k_c}{k}, kR\right)}. \tag{22}$$

The δ-shell potential can at most exhibit one bound state. It is interesting to identify the critical strength λ_* at which the bound state enters. To do so, we start from Eq. (21), and consider a resonance by setting $\delta = \pi/2$. In order to take the limit $k \to 0$, we employ asymptotic approximations of the Coulomb wave functions (see Appendix for details). This yields

$$\lambda_*^{-1} = -2RI_1\left(2\sqrt{2k_cR}\right)K_1\left(2\sqrt{2k_cR}\right). \tag{23}$$

Here, I_1 and K_1 are modified Bessel functions.

The effective range-expansion for the δ-shell potential is [7, 49]

$$\begin{aligned} a_l^{-1} &= \frac{2k_c^{2l+1}}{\left(l!I_{2l+1}\right)^2}\left(\frac{1}{\lambda_0 R} + 2I_{2l+1}K_{2l+1}\right) \\ r_l &= -\frac{2k_c^{2l-1}}{3\left(l!I_{2l+1}\right)^2}\Bigg[2\frac{k_c}{\lambda_0}\frac{lI_{2l+3} + \sqrt{2k_cR}I_{2l+2}}{I_{2l+1}} \\ &\quad +2l(l+1)(l+2)I_{2l+1}K_{2l+1} \\ &\quad -\frac{1}{2}\left(I_{2l+1}\right)^2 - l(l+1) - k_cR\Bigg]. \end{aligned} \tag{24}$$

Here, we used the shorthands

$$I_l \equiv I_l\left(2\sqrt{2k_cR}\right) \tag{25}$$

for the modified Bessel functions.

3. Resonances

As λ_0 is decreased from 0 at fixed R, the potential becomes increasingly more attractive. Just before the critical strength (23) is reached, the phase shift exhibits a quick rise through $\pi/2$ at a low momentum κ. This is reminiscent of a resonance, and we can indeed model this physical phenomenon. The goal is to adjust the parameters of the δ-shell potential to the resonance energy and width. To do so, we set $\delta = \pi/2$ in Eq. (21) and find

$$\frac{\kappa}{\lambda_0} = -F_l\left(\frac{k_c}{\kappa}, \kappa R\right)G_l\left(\frac{k_c}{\kappa}, \kappa R\right). \tag{26}$$

This relates the parameters of our potential to the resonance momentum κ. The resonance energy is $E_\kappa = \hbar^2\kappa^2/(2m)$. To compute the resonance width Γ, we use the relation [52]

$$\left.\frac{d\delta}{dE}\right|_{E_\kappa} = \frac{2}{\Gamma}. \tag{27}$$

This relation is particularly useful because it allows us to describe narrow resonances based on elastic scattering phase shifts [53]. We denote the momentum derivative of a function f as $\frac{df}{dk} \equiv \dot{f}$, take the derivative with respect to momentum of Eq. (21), and set $\delta = \pi/2$. This yields

$$\lambda_0^{-1} = (F_l)^2 \dot{\delta} - \dot{F}_l G_l - F_l \dot{G}_l. \tag{28}$$

Here and in what follows we suppress the arguments $(k_c/\kappa, \kappa R)$ of the Coulomb wave functions. Combining Eqs. (26) and (28), and using $\dot{\delta} = 4E_\kappa/(\kappa\Gamma)$ yields an expression for the width that depends on R alone (and not on λ_0)

$$\frac{E_\kappa}{\Gamma} = \frac{\kappa\left(\dot{F}_l G_l + F_l \dot{G}_l\right) - F_l G_l}{4(F_l)^2}. \tag{29}$$

Given the width and the resonance energy, one can solve Eq. (29) for the parameter R; substitution of the result into Eq. (26) then yields the parameter λ_0.

It is now interesting to combine the result (26) with Eq. (21) to compute the phase shift. We find

$$\cot\delta = \frac{\frac{k}{\kappa} F_l\left(\frac{k_c}{\kappa}, \kappa R\right) G_l\left(\frac{k_c}{\kappa}, \kappa R\right) - F_l\left(\frac{k_c}{k}, kR\right) G_l\left(\frac{k_c}{k}, kR\right)}{F_l^2\left(\frac{k_c}{k}, kR\right)}. \tag{30}$$

Here, it is implied that R fulfills Eq. (29).

C. Systematic improvements

We want to make systematic improvements to the δ-shell potential. For this purpose, let us recall how this is accomplished in pion-less EFT. There, the leading-order is a contact potential, e.g. a δ-shell potential with a range R that is much smaller than any other length scale in the problem under consideration. Then, leading corrections for s-waves are of the form

$$g\Delta\delta(r - R^+) + g\delta(r - R^+)\Delta. \tag{31}$$

Here, Δ is the Laplacian, and g is a coupling constant. When acting on the wave function with energy $E_k = \hbar^2 k^2/(2m)$ of the leading-order Hamiltonian the perturbation (31) yields a contribution proportional to gk^2, and this is a small correcton because $g \propto R^2$ in a natural EFT, and $kR \ll 1$ because k is a low momentum and R is a small length scale.

Having this in mind, we now have to consider our case, i.e. Coulomb is added. Let us discuss how to make systematic improvements to the δ-shell potential. For this purpose we consider the operator

$$W_n \equiv \frac{1}{2}(H_0)^n \delta(r - R^+) + \frac{1}{2}\delta(r - R^+)(H_0)^n. \tag{32}$$

Here, R^+ denotes a point that is larger than R by an arbitrarily small amount, and n is a non-negative integer [1]. Consider the Hamiltonian ($n \geq 1$)

$$\tilde{H}_n = H_0 + V + g_n W_n, \tag{33}$$

where g_n denotes a low-energy constant. We write down the Schrödinger equation for the Hamiltonian $\tilde{H}_n$ acting on the eigenfunction of H_0 with eigenvalue E and integrate over the neighborhood of the singularities at $r = R$. This yields

$$\begin{aligned} 0 &= \int_{R^-}^{R^+} dr \tilde{H}_n u_l(r) \\ &= -\frac{\hbar^2}{2m}\left[u_l'(R^+) - u_l'(R^-) - \lambda_0 u_l(R)\right] + g_n E^n u_l(R^+) \end{aligned} \tag{34}$$

Comparison with Eq. (14) shows that the matching condition becomes

$$u_l'(R^+) - u_l'(R^-) = \tilde{\lambda} u_l(R), \tag{35}$$

where we introduced the energy-dependent coupling constant

$$\tilde{\lambda} \equiv \lambda_0 + \frac{2m}{\hbar^2} g_n E^n. \tag{36}$$

One might prefer to convert energy dependence into a momentum dependence. We employ the shorthand

$$g_n = \left(\frac{2m}{\hbar^2}\right)^{n-1} \tilde{g}_n, \tag{37}$$

and $E = \hbar^2 k^2/(2m)$, noting that k can be real (for positive energies) or purely imaginary $k = i\gamma$ for bound states. Then, the momentum-dependent coupling constant is

$$\tilde{\lambda}(k) = \lambda_0 + \tilde{g}_n k^{2n}. \tag{38}$$

We remind ourselves that this is only correct if the Hamiltonian acts on eigenstates of H_0.

Let us discuss the power counting. The breakdown momentum is Λ_b. By definition, the leading-order Hamiltonian (11) and the perturbation (32) have the same energy $\hbar^2\Lambda_b^2/(2m)$ at the breakdown scale. Equating the respective energies yields

$$\frac{\hbar^2\Lambda_b^2}{2m} \sim \frac{\hbar^2\Lambda_b^2}{2m}^n g_n |u_l(R)|^2. \tag{39}$$

Using the estimate $|u_l(R)|^2 \sim R^{-1}$ yields the scaling

$$\tilde{g}_n \sim \frac{R}{\Lambda_b^{2(n-1)}}. \tag{40}$$

[1] We could envision also more "democratic" ways to write powers of H_0 left and right from the δ function, but this is not important at this stage.

Thus, for "natural" coefficients of this size, the momentum-dependent coupling constant (38) is a small correction at low momenta, and contributions systematically decrease with increasing n. We propose that W_2 is the leading correction to the Hamiltonian H. The rationale is as follows: The two parameters of our theory allow us to fit, for instance, the scattering length and the effective range. Then, a quartic correction at next-to-leading order should affect the shape parameters in the effective range expansion.

We note that the same result could have been obtained from perturbation theory. We also note that the same systematic corrections apply to the Breit model or the square-well potential. The reason is that also for these models the eigenstates of $H = H_0 + V$ are wave functions of the "free" Hamiltonian H_0 for $r > R$. Thus, the expectation value of $g_n W_n$ in a state with low energy $E = \hbar^2 k^2/(2m)$ is $(k^2/\Lambda_b^2)^{n-1} E$. For $k \ll \Lambda_b$, this is a small correction and we have established a power counting. The systematically improvable Hamiltonian is (with terms in order of decreasing importance)

$$\begin{aligned} H &= H_0 + \frac{\hbar^2 \lambda_0}{m} W_0 + g_2 W_2 + g_3 W_3 + \dots \\ &= H_0 + \frac{\hbar^2 \lambda(k)}{m} \delta(r - R) \end{aligned} \tag{41}$$

In the first line, we have replaced the δ-shell potential (13) by W_0. In the second line we reminded ourselves that this corresponds to introducing a momentum-dependent coupling constant

$$\lambda(k) = \lambda_0 + \tilde{g}_2 k^4 + \tilde{g}_3 k^6 + \dots \tag{42}$$

when acting on eigenstates of $H = H_0 + V$. In what follows, we will simply denote the coupling constant as λ, suppressing its momentum dependence. In practical applications, we will use $\lambda = \lambda(0) = \lambda_0$, and employ the leading correction to estimate systematic uncertainties.

On the one hand, the proposed way to include corrections to the δ-shell Hamiltonian (11) exhibits a power counting and thereby follows central ideas from EFT. On the other hand, the approach is not simply a derivative expansion of the unknown strong interaction, because H_0 contains the Coulomb potential. This is important, because the contributions from the Coulomb potential and the kinetic energy are large when the Sommerfeld parameter is large; only the combination of kinetic and Coulomb potential energy yields a small total energy. To see this, we note that the expectation value of the Coulomb potential term $\delta(r - R^+)\hbar^2 k_c/(mr)$ for a state with energy E is $C_l^2 \hbar^2 k_c/(mR)$. As this expectation value can be very large (compared to $C_l^2 E$), the contribution of a derivative contact such as $\delta(r - R^+)\hbar^2 \Delta/(2m)$ must be large in size, too, when compared to $C_l^2 E$. This analysis suggests that systematic improvements to Coulomb systems should be based on a Coulomb-corrected derivative expansion such as Eq. (41), rather than on a purely derivative expansion as done in Coulomb halo EFT.

Nucleus	J^π	l	λ_0 (fm^{-1})	R (fm)
^{6}Li	1^+	0	-0.89	3.84
^{7}Li	$3/2^-$	1	-1.45	3.14
^{7}Li	$1/2^-$	1	-1.31	3.50
^{7}Be	$3/2^-$	1	-1.42	3.22
^{7}Be	$1/2^-$	1	-1.25	3.75
^{17}F	$5/2^+$	2	-1.63	3.60
^{17}F	$1/2^+$	0	-0.79	3.85
^{8}Be	0^+	0	-0.81	3.54

TABLE III. Potential parameters (λ_0, R) of the δ-shell potential that reproduce the central values for the nuclei described in this paper.

To further illuminate this point, we consider the Coulomb wave functions $F_0(k_c/k, kr)$ and $G_0(k_c/k, kr)$ for the case of low momentum (i.e. for $k \to 0$) and large Coulomb momentum (i.e. for $k_c r \gg 1$). Then (details are presented in the Appendix)

$$\begin{aligned} \frac{d}{dr} F_0(k_c/k, kr) &\approx +4 k_c F_0(k_c/k, kr), \\ \frac{d}{dr} G_0(k_c/k, kr) &\approx -4 k_c G_0(k_c/k, kr). \end{aligned} \tag{43}$$

Thus, the derivative of the Coulomb wave function (even with a small momentum $k \ll k_c$) yields the large Coulomb momentum k_c. This casts some doubts on employing the usual derivative expansion known from pionless EFT when the Coulomb momentum is large compared to the momentum scale of interest.

III. RESULTS

In this Section we present our results for various systems of interest. Our emphasis is on uncertainty estimates and a comparison with results from Coulomb halo EFT. The prediction of the ^{17}F charge radius is subject to confrontation with data [54]. For completeness, we display the parameters of the δ-shell potential in Table III. We note that the values of D (i.e. the sum of the ions' charge radii) in Table II are smaller than the values of R displayed in Table III (except for the $3/2^-$ ground state of ^{7}Li). Thus, the strong interaction is peripheral in the cluster model we employ. In what follows we will employ energies of bound and resonant states. These are all taken from National Nuclear Data Center [55].

A. ^{8}Be as $\alpha + \alpha$ resonance

The nucleus ^{8}Be is not bound, but rather a $J^\pi = 0^+$ resonant state at an energy $E \approx 92$ keV and a width of $\Gamma \approx 6$ eV above the $\alpha + \alpha$ threshold. The next known 0^+ state is at 20.2 MeV of excitation. We note that this energy is equal to the energy of the first 0^+ state of the α particle to three significant digits. Assuming there are indeed no other 0^+ states, 20 MeV sets the empirical

breakdown energy for any cluster model or EFT that describes ^{8}Be in terms of "elementary" α particles (because an "elementary" point particle dies not exhibit any structure and cannot be exited). The corresponding empirical breakdown momentum is 1.4 fm^{-1}.

However, α particles have a finite size, and the sum of the two charge radii of the α particles is $D \approx 3.3$ fm. At a momentum $\pi/D \approx 0.95$ fm^{-1}, the details of any Hamiltonian with a physical range D can be resolved. The corresponding breakdown energy in the center-of-mass system is $E_b \approx 9.4$ MeV. This energy is lower than the empirical breakdown scale discussed in the previous paragraph and therefore sets the breakdown scale. We note that it is not precluded to construct a model that describes data accurately even at the breakdown scale. However, that would seem to be fortuitous, as a generic finite-range model that is adjusted to low-energy data is expected to not be accurate at such energies.

The Coulomb momentum is $k_c \approx 0.28$ fm^{-1}. We expect model dependencies to become visible above the momentum $\Lambda_m \approx 0.4$ fm^{-1}, see Eq. (10). This corresponds to a center-of-mass energy of about $E_m = \hbar^2\Lambda_m^2/(2m) \approx 1.7$ MeV. Recall that this is the energy where the classical turning point is at a radial distance D.

To summarize the arguments: Virtually any model with a physical range of size D that is adjusted to low-energy data is expected to describe data accurately up to about $E_m = 1.7$ MeV. At higher energies, model dependencies start getting resolved because the strong potential is not anymore in the classically forbidden region; a de-facto breakdown of models with a range of size D is expected at an energy of about $E_b = 9.4$ MeV. The model dependencies of the δ-shell potential can be estimated by employing the momentum dependent coupling $\lambda(k) = \lambda_0 + gRk^4/\Lambda_b^2$. Here, g is a number of order one.

Figure 1 shows s-wave phase shifts for $\alpha - \alpha$ scattering computed from different models, and compares them to data. The two-parameter models have been adjusted to the resonance energy and its width. The models are (i) the δ-shell potential, (ii) a shallow square well (with no bound states), (iii) a deep square well with multiple bound states[2], and (iv) the Breit model [48], i.e. a hard-core potential where the wave function's logarithmic derivative at the hard core is set. All models are practically indistinguishable below $E_m \approx 1.7$ MeV and differ significantly at the breakdown energy $E_b \approx 9.4$ MeV. This behavior is as expected from the discussion of the energy scales presented in Sect. II A 2. We note that the δ-shell potential and the Breit model yield similar results. However, unlike the former, the latter employs a hard core and its wave functions thus exhibit significant high-momentum modes.

Let us focus on the δ-shell potential and estimate uncertainties. Figure 2 shows the phase shifts over an even larger range of energies. The central line is obtained from adjusting to the resonance energy and the central value of its width. Varying the resonance width $\Gamma = 5.57 \pm 0.25$ eV within its uncertainty produces the dark band. The systematic uncertainty estimate, i.e. the range that different models would explore, is shown as a light band. Its extent is generated by employing $\lambda(k) = \lambda_0 \pm Rk^4/\Lambda_b^2$. We see that the prediction of the δ-shell potential agrees well with data, even for energies beyond $E_m = 1.7$ MeV. This model happens to be accurate. The comparison with Fig. 1 shows that the systematic uncertainty band is a reasonable estimate for the range of results spanned by different models.

We computed the scattering length and effective range and obtained $a_0 = -2020 \pm 100$ fm and $r_0 = 1.106 \pm$

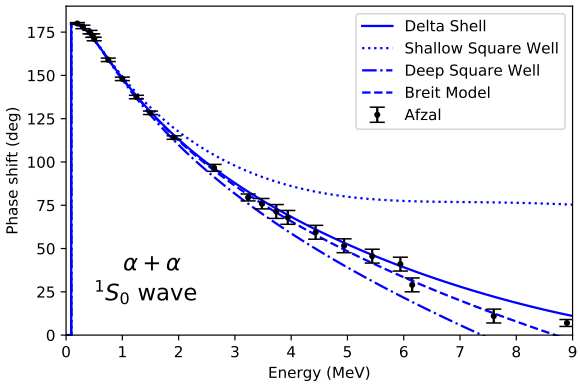

FIG. 1. (Color online) Phase shifts of $\alpha - \alpha$ scattering in the s wave, as a function of the center-of-mass energy computed with a shallow square-well potential (dotted line), the δ-shell (solid line), the Breit model (dashed line) and a deep square well (dashed-dotted line). Data taken from Refs. [56, 57].

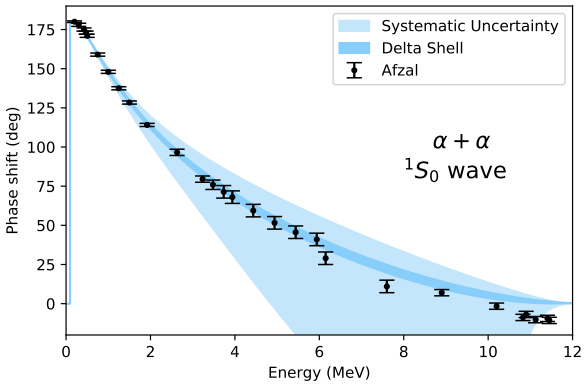

FIG. 2. (Color online) Phase shifts of $\alpha - \alpha$ scattering in the s wave, as a function of the energy in the center-of-mass frame. The dark band shows the uncertainty from the resonance width. The light band shows the theoretical uncertainty estimate. Data taken from Refs. [56, 57].

[2] These bound-state energies are large and outside the domain of low-energy physics.

0.005 fm, respectively. The uncertainties stem from the uncertainty in the resonance width. Let us compare this with effective range parameters from the literature. Overall, there is a consensus on the effective range, which is close to the estimate $1/(3k_c) = 1.21$ fm shown in Table I. The scattering length, of course, is sensitive to the precise difference $r_0 - 1/(3k_c)$ [see the approximation (7)], and it is probably only known to about 5 to 10%. The effective range expansions by Rasche [58], Higa *et al.* [13], and Kamouni and Baye [59] found $a_0 = 1650 \pm 150$ fm, $a_0 = 1920 \pm 90$ fm, and $a_0 = 2390$ fm, respectively. The potential models by Kulik and Mur [3] yielded $a_0 = 2030 \pm 100$ fm. Ab initio computations have not yet reached the precision to extract very large scattering lengths precisely [60].

We discuss some of these works in more detail. Kulik and Mur [3] uses simple models for the computation of phase shifts and effective range parameters. The two-parameter models are the δ-shell potential and the Breit model. These models are adjusted to the resonance energy and to phase shifts, and they virtually agree with each other for energies in the center-of-mass system up to 2 MeV. They agree with data over an even wider range. Interestingly, these models yield an accurate description of the resonance width when adjusted to phase shifts. Kamouni and Baye [59] use the resonating group method and R-matrix theory to extract an effective range expansion. This approach adjusts about two parameters in each partial wave.

Let us also contrast our approach to the halo EFT work by Higa *et al.* [13]. That approach is based on a dimeron formulation with contact interactions. At leading order (LO), a fit to the resonance energy and width yields phase shifts that agree with data only up to 0.3 MeV in the center-of-mass frame. At next-to-leading-order (NLO), three parameters are adjusted to the resonance energy, its width, and phase shifts. The resulting phase shifts clearly deviate from data above 0.7 MeV of center-of-mass energy. Figure 3 compares the EFT results at LO and NLO to models. The EFT results are not accurate. This is somewhat surprising, because the effective-range expansion by the same authors yielded phase shifts that agree with data.

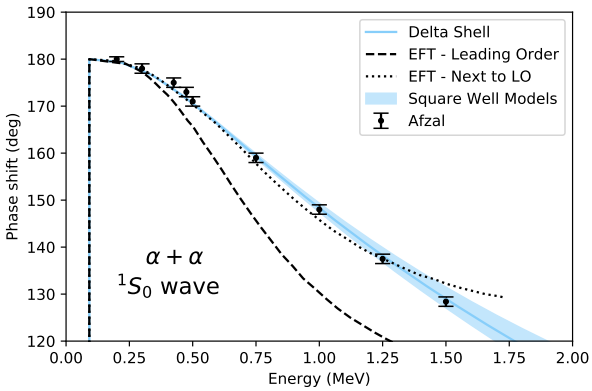

FIG. 3. (Color online) Phase shifts of $\alpha + \alpha$ scattering in the s wave computed from finite-range models and in leading order (LO) and next-to-leading order (NLO) Coulomb halo EFT [13], as a function of the center-of-mass energy. Data taken from Refs. [56, 57].

B. ^{17}F as ^{16}O + p

The ^{17}F nucleus plays a role in nucleosynthesis. Its $J^\pi = 5/2^+$ ground state and its first excited $1/2^+$ states are bound by about 0.6 and 0.1 MeV, respectively. These energies are small compared to 6 MeV, the energy it takes to excite the doubly-magic nucleus ^{16}O, and we can thus approximate ^{17}F as a ^{16}O+p system at sufficiently low energies. The next excited states in ^{17}F with quantum numbers $5/2^+$ and $1/2^+$ are separated by 6.7 and 6.5 MeV, respectively, from the corresponding bound states. Thus, the empirical breakdown energy is about $E_b \approx 6$ MeV. The sum of the charge radii of the proton and ^{16}O is about $D \approx 3.6$ fm. This sets the theoretical breakdown momentum to $\pi/D \approx 0.88$ fm^{-1}, corresponding to an energy of about 17 MeV. Thus, the breakdown scale is set by the empirical breakdown energy. The Coulomb momentum is $k_c \approx 0.26$ fm^{-1}. Thus, potentials with a physical range D are expected to exhibit model dependencies above about $\Lambda_m = (2k_c/D)^{1/2} \approx 0.27$ fm^{-1}, corresponding to an energy $E_m \approx 1.6$ MeV.

Let us consider the excited $J^\pi = 1/2^+$ halo state [61]. We adjust the model parameters to the binding energy and the $^2S_{1/2}$ phase shift data from Ref. [62]. The results are shown in Fig. 4. We then predict the ANC to be $C_0 = 78.9 \pm 4.2$ fm$^{-1/2}$, and the charge radius of the excited state is $R_c^* = 3.096 \pm 0.034$ fm. The uncertainties reflect the uncertainties from the χ^2 fit of the phase shifts, obtained from doubling the χ^2. The ANC agrees with the results by Gagliardi *et al.* [46], Artemov *et al.* [47], and Huang *et al.* [26], who found values of (80.6 ± 4.2) fm$^{-1/2}$, (75.5 ± 1.5) fm$^{-1/2}$, and 77.2 fm$^{-1/2}$, respectively. Our effective range parameters are $a_0 = 4080 \pm 430$ fm, and $r_0 = 1.17 \pm 0.01$ fm. Within their uncertainties, these values agree with those of Refs. [10, 59].

Let us also compare to Coulomb halo EFT. For the excited $1/2^+$ state, Ryberg *et al.* [14] employed one parameter at leading order and found that the relative distance $\langle r^2 \rangle = (0.59 \text{ fm})^2$ between the proton and the core and the ANC $C_0 = 21.4$ fm$^{-1/2}$ are too small. At next-to-leading order, effective range contributions enter, and the charge radius is increased by a factor 3.6–3.8 [65].

Let us turn to the ^{17}F ground state. Its charge radius is not yet known but its measurement is currently an active experiment at CERN Isolde [54]. We want to make a prediction for this observable. To put things into perspective we note that the charge radius of ^{19}F is $R_c = 2.8976(25)$ fm [66]; the ground-state of that nucleus has spin/parity $1/2^+$. We adjust our model

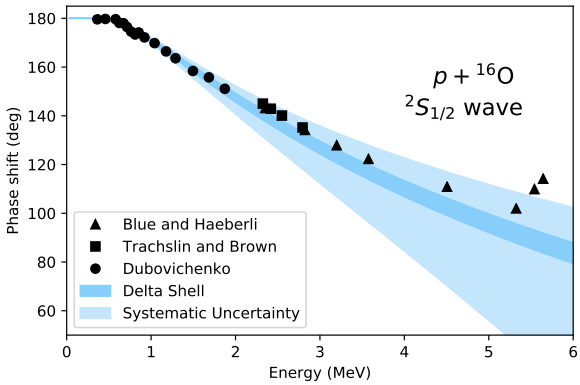

FIG. 4. (Color online) Phase shifts of $p + {}^{16}$O scattering in the $^2S_{1/2}$ partial wave, as a function of the energy in the center-of-mass frame. Data taken from Ref. [62–64].

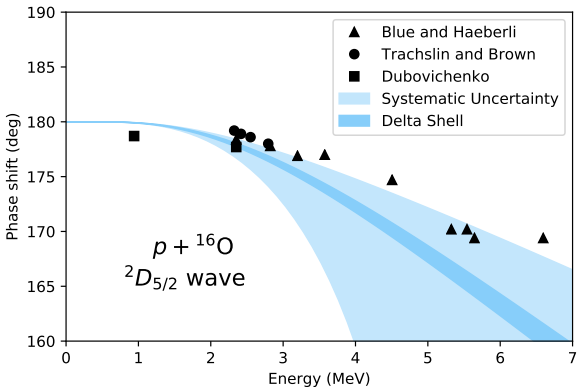

FIG. 5. (Color online) Phase shifts of $p + {}^{16}$O scattering in the $^2D_{5/2}$ partial wave, as a function of the energy in the center-of-mass frame. Data taken from Refs. [62–64].

parameters to the binding energy and the ANC. The ground-state ANC extracted from transfer reaction data via potential models is 1.04 ± 0.05 fm$^{-1/2}$ [46, 47]. The resulting phase shifts are shown in Fig. 5. Unfortunately, the phase shift analysis lacks uncertainties, but we see a systematic deviation. We compute a scattering length of $a_2 = 1.15(11) \times 10^3$ fm^5 and an effective range of $r_2 = -0.068(7)$ fm^{-3}, in agreement with results by Yarmukhamedov and Baye [10] (who were also informed by the ANCs we used). We compute a charge radius of $R_c = 2.88(1)$ fm. This is a large radius for a d-wave state and practically as large as the charge radius of the $1/2^+$ ground state of ^{19}F.

To estimate the reliability of our computations, we alternatively fit to the potential parameters to the phase shifts and the binding energy and find $R \approx 2.957$ fm and $\lambda_0 \approx -1.924$ fm^{-1}. We note the the resulting χ^2 per degree of freedom is about 11, hinting at phase-shift uncertainties of about three degrees (assuming them to be of statistical nature). In this case, we compute an ANC of $C_2 = 0.7286$ fm$^{-1/2}$, and a charge radius $R_c = 2.80(2)$ fm. These values are significant smaller than those given in the previous paragraph, and the uncertainties do not overlap. It seems to us that the phase shift data [62–64] and the transfer reaction data [46] are probably not compatible. We note, however, that the accurate determination of d-wave phase shifts from low-energy scattering is complicated because s and p waves dominate. We also note that somewhat smaller ANCs of 0.91 and 0.88 fm$^{-1/2}$ have been computed by Huang *et al.* [26] and Blokhintsev *et al.* [12], respectively. As the extraction of the ANC by Gagliardi *et al.* [46] is more recent than the phase shift analysis (and includes uncertainties), we base our computation on the ANC and predict a charge radius of 2.88(1) fm for ^{17}F. The measurement [54] will certainly be useful to yield insight into the low-energy properties of the $p + {}^{16}$O system. We also note that this nucleus is in reach of ab initio computations [67], but its charge radius and ANC have not been computed, yet.

C. ^{6}Li as a $\alpha + d$ bound state

The ground state of ^{6}Li is only bound by about $E = 1.47$ MeV with respect to the $d + \alpha$ threshold. This corresponds to a bound-state momentum of $\gamma \approx 0.31$ fm^{-1}. Its spin/parity is identical to that of the deuteron, and the estimate (5) for its magnetic moment yields 0.86 nuclear magnetons, which is close to the observed value of 0.822 [68]. These basic properties suggest that the ^{6}Li ground state exhibits a dominant s-wave halo structure, and we will we neglect any d-wave component in what follows.

Let us assess the breakdown scale. The three-body breakup of ^{6}Li into $\alpha + n + p$ requires the breakup of the deuteron and is thus about 2.2 MeV above threshold. This inelastic process is without concern to us. The first excited state with the same spin and parity as the ground state is at 5.65 MeV, and this is the empirical breakdown energy. The sum of charge radii is $D \approx 3.8$ fm, setting the theoretical breakdown momentum at $\pi/D \approx 0.82$ fm^{-1}, which corresponds to a high energy of 10.6 MeV. Thus, the breakdown scale is set by the empirical properties. The binding energy of the deuteron to the α core is a factor of about four smaller than the breakdown energy, and this provides us with a separation of scale. The Coulomb momentum of the $d + \alpha$ system is $k_c \approx 0.09$ fm^{-1}, and model differences are start to get resolved above the momentum $\Lambda_m \approx 0.22$ fm^{-1}, corresponding to an energy $E_m \approx 0.75$ MeV. As this energy is smaller than the binding energy of the $\alpha + d$ system, model dependencies could be relevant. However, below we will see that the δ-shell model yields an accurate description of existing low-energy data.

We model the ^{6}Li ground state using the δ-shell poten-

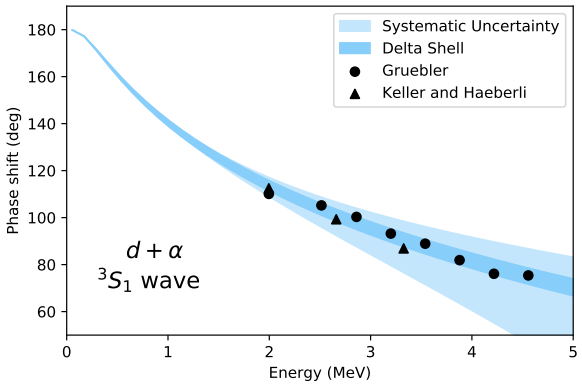

FIG. 6. (Color online) Phase shifts of $d + \alpha$ scattering in the $^3S_1$ partial wave, as a function of the energy in the center-of-mass frame. Data taken from Refs. [70, 71].

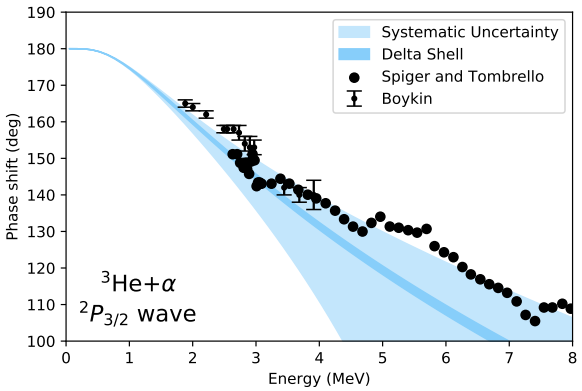

FIG. 7. (Color online) Phase shifts of $^3\mathrm{He} + \alpha$ scattering in the $^2P_{3/2}$ partial wave, as a function of the energy in the center-of-mass frame. Data taken from Refs. [78, 79]

tial in the s partial wave. Ryberg *et al.* [69] pointed out that charge radii can be used to constrain low-energy observables that are relevant in astrophysics. Together with the binding energy, these are the most precise data available at low energies. We therefore adjust the two parameters of our potential to the binding energy and the charge radius. The charge radius of ^{6}Li is 2.589 ± 0.039 fm [66] and we perform a total of three calculations, adjusting to its central, lower, and upper values. For the relevant s wave we compute an ANC of $C_0 = 2.23(11)$ fm$^{-1/2}$, a scattering length $a_0 = 29.1 \pm 1.7$ fm, and an effective range $r_0 = 1.85(5)$ fm. The uncertainties reflects the uncertainty in the charge radius. The central value of the inter-ion distance is $\sqrt{\langle r^2 \rangle} = 3.86$ fm, and this marginally exceeds the sum of charge radii of its constituents, 3.82 fm. The resulting phase shifts are shown in Fig. 6, and they agree with data [70, 71]. This gives us confidence in the accuracy of our results.

It is interesting to compare our prediction for the ANC and the effective range parameters with the literature. The effective range parameters agree with Ref. [72], which states $a_0 = 30.8$ fm and $r_0 = 1.88$ fm; the ANC agrees with the values of Refs. [5, 73, 74]. However, we note that ANCs have clearly evolved (and decreased) over time, as the papers [73, 75–77] show. We note that the ab initio computation by Nollett *et al.* [20] reports an ANC of 2.28 ± 0.02 fm$^{-1/2}$ (in agreement with recent cluster models and our result), while Hupin *et al.* [22] found a larger ANC of about 2.7 fm$^{-1/2}$. While the calculation of Ref. [20] is informed by charge radii through its variational wave function, the paper [22] did not present results for charge radii. We believe our calculations, through their consistency for all low-energy observables, add further weight to an ANC around 2.2 fm$^{-1/2}$.

D. ^{7}Be as $\alpha + ^3$He bound state

The ^{7}Li ground state has quantum numbers $J^\pi = 3/2^-$ and is bound by 1.6 MeV with respect to the $\alpha + ^3$He threshold. The only other bound state is at about 0.4 MeV of excitation energy and has quantum numbers $J^\pi = 1/2^-$. Both states are thus weakly bound and can be viewed as p waves of the $\alpha + ^3$He system. We note that the estimate (5) for the ground state's magnetic moment, -1.556 nuclear magnetons, is close to the experimental value of -1.398 [68]. This all suggests that we can describe ^{7}Be as an $\alpha + ^3$ He system.

The empirical breakdown energy is set by the energy of excited states 9.9 MeV for quantum numbers $J^\pi = 3/2^-$; it is about twice as high for the numbers $J^\pi = 1/2^-$ state. Of course, the ^{3}He nucleus breaks up at an excitation energy of about 6 MeV, but this inelastic channel is of no concern for us. The sum of the two charge radii is $D \approx 3.6$ fm, setting the theoretical breakdown momentum to $\pi/D \approx 0.86$ fm^{-1}, corresponding to an energy of 9 MeV. Thus the breakdown energy is about 9 MeV. Model dependencies become visible above the momentum scale $\Lambda_m \approx 0.36$ fm^{-1}, corresponding to an energy of 1.6 MeV. We note that this energy is similar to the ground-state energy.

For the $^2P_{3/2}$ partial wave, we adjust the two parameters of the δ-shell potential to the binding energy of the ground state and its charge radius of 2.646 ± 0.016 fm [66]. As before, we propagate the uncertainty of the charge radius to low-energy observables. Then, the ground-state ANC is $C_1 = 3.6 \pm 0.1$ fm$^{-1/2}$, and the effective-range parameters are $a_1 = 207 \pm 8$ fm^3 and $r_1 = -0.041 \pm 0.004$ fm^{-1}. The predicted phase shifts are shown in Fig. 7 and compared to data [78, 79]. The agreement is fair. Unfortunately, the older data by Spiger and Tombrello [78] lacks uncertainties.

Let us compare with other approaches for the $3/2^-$ partial wave. Descouvemont *et al.* [25] found an ANC

of $C_1 = 3.79$ fm$^{-1/2}$ (close to our value) from an R matrix analysis, while Tursunmahatov and Yarmukhamedov [80] found an ANC of $C_1 = 4.83^{+0.1}_{-0.25}$ from evaluations of capture reactions. We refer to the latter paper for a review of literature values. The ab initio computation by Dohet-Eraly *et al.* [23] found a scattering volume of $a_1 = 210.4$ fm^3 (close to our result), while the effective range expansion techniques [10] found effective range parameters $a_1 = 301 \pm 6$ fm^3 and $r_1 = 0.0170 \pm 0.0026$ fm^{-1} (and a squared ANC of $C_1^2 = 23.3$ fm^{-1}). We note that the ab initio computation [23] yields a charge radius that is close to data.

We note that Coulomb halo EFT was very recently applied to the $\alpha + {}^3$He system [16, 18] for a computation of the astrophysical S factor. Zhang *et al.* [18] pursued a Bayesian approach based on data from capture reactions, avoiding the need to adjust parameters to phse shifts. Higa *et al.* [16] employed the ANC from Ref. [80] for their computation of the astrophysical S factor. At leading order (a one-parameter or a three-parameter theory, depending on the power counting), the resulting phase shifts are visibly above the data [79].

It seems to us that this $\alpha + {}^3$He system is still not sufficiently well understood. Existing theoretical results are in conflict with each other, and no calculation seems to be able to reproduce charge radii, phase shifts, and capture data.

E. ^{7}Li as $\alpha + {}^3$H bound state

The $3/2^-$ ground state of ^{7}Li is bound by about 2.5 MeV with respect to the threshold of the $\alpha + {}^3$H system. Based on a cluster assumption (5), its magnetic moment is 3.4 nuclear magnetons, which is close to the experimental datum of 3.256 [68]. This suggests that one can describe ^{7}Li as the bound state of the $\alpha + {}^3$H system with orbital angular momentum $l = 1$.

The next $3/2^-$ state is at about 9.8 MeV, setting the empirical breakdown scale. The breakup of the triton at about 6 MeV is an inelastic channel we are not concerned with. The sum of the charge radii of the constituent ions is $D \approx 3.4$ fm, and the theoretical breakdown momentum is $\pi/D \approx 0.91$ fm^{-1}, corresponding to an energy of about 10 MeV. Thus the breakdown energy is at about 10 MeV. At the momentum $\Lambda_m = 0.26$ fm^{-1}, corresponding to an energy of 0.84 MeV, model dependencies become visible. We note that this energy is smaller than the bound-state energy, and model dependencies could thus be notable.

We adjust the δ-shell parameters to the α-separation energy and the charge radius (2.444 ± 0.042 fm [66]) of the ^{7}Li. The resulting phase shifts are shown in Fig. 8 and compared to a phase shift analysis [78]. The agreement is poor. However, the scatter of the points from the phase shift analysis also suggests that the uncertainties are significant.

For the $3/2^-$ channel, we compute a scattering volume $a_1 = 74 \pm 8$ fm^3, an effective range $r_1 = -0.24 \pm 0.02$ fm^{-1}, and an ANC $C_1 = 3.0 \pm 0.2$ fm$^{-1/2}$. The ab initio computations by Dohet-Eraly *et al.* [23] found a scattering volume of 70 fm^3 (which agrees with our result), and their computed charge radius is close to data. Kamouni and Baye [59] fit a model to phase shifts and report effective-range parameters $a_1 = 72.77$ fm^3 and $r_1 = 0.27$ fm^{-1} (which are close to our results); however, the ground-state energy of the ${}^3\mathrm{H} + \alpha$ system was about twice as large as the data. However, Descouvemont *et al.* [25] found an ANC of $C_1 = 3.49$ fm$^{-1/2}$ from an R matrix analysis, while Yarmukhamedov and Baye [10] computed effective-range parameters $a_1 = 58.10 \pm 0.65$ fm^3 and $r_1 = 0.346 \pm 0.005$ fm^{-1} (with an ANC of $C_1 = 3.57 \pm 0.15$ from Ref. [81]).

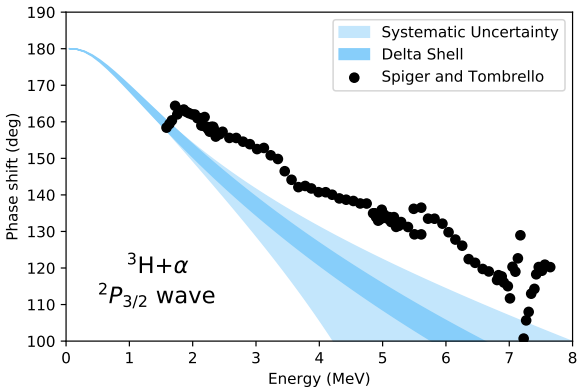

FIG. 8. (Color online) Phase shifts of ${}^3\mathrm{H} + \alpha$ scattering in the ${}^2P_{3/2}$ partial wave, as a function of the energy in the center-of-mass frame. Data taken from Ref. [78].

We see that there is no consensus yet about low-energy observables for the $\alpha + {}^3$H system. However, the simplicity of the δ-shell potential, its economical use of only two low-energy data, its agreement with ab initio computations, and its ability to estimate uncertainties of models make it an attractive potential also here.

IV. SUMMARY

We employed a simple two-parameter model to describe a number of nuclear light-ion systems that exhibit a separation of scale. Whenever possible, the model parameters were constrained by the energy and width of a low-energy resonance or by the energy and charge radius of a weakly bound state. In those cases, we predicted phase shifts, effective range parameters and ANCs. Our analysis of ANCs, charge radii and resonance widths shows that the inclusion of a finite range is relevant for systems with strong Coulomb interactions. We also proposed a way to account for systematic corrections and model uncertainties. This allowed us to present uncertainty estimates for the computed observables. The presented approach provides us with a constructive criticism

of Coulomb halo EFT. We predicted a charge radius of 2.88(1) fm for the ^{17}F ground state, taking its energy and ANC to constrain the model.

The potential model employs two parameters in each partial wave. When applied to a single partial wave, it is a minimal model whose results compete well at low energies with traditional Woods-Saxon potential models or R matrix analyses that employ more parameters. We pointed out that the δ-shell model practically delivers model-independent results below a momentum Λ_m when it is adjusted to low-energy data. We also presented simple formulas that estimate the sizes of effective-range parameters and ANCs based on energies of low-energy states and charge radii of the involved ions. Such estimates are useful in the construction of EFTs, and they seemed to be missing in the literature.

ACKNOWLEDGMENTS

We are indebted to Lucas Platter for many stimulating and insightful discussions. We also thank Hans-Werner Hammer, Sebastian König, Titus Morris, and Daniel Phillips for useful discussions; Chenyi Gu for pointing out a numerical problem with Coulomb wave functions, and Petr Navrátil for providing us with data. We thank the Institute for Nuclear Theory at the University of Washington for its hospitality and the U.S. Department of Energy for partial support during the completion of this work. This work has been supported by the U.S. Department of Energy under grant Nos. DE-FG02-96ER40963, and DE-SC0016988, and contract DE-AC05-00OR22725 with UT-Battelle, LLC (Oak Ridge National Laboratory).

V. APPENDIX

The Appendix presents some details that could be looked up or are straightforward (but sometimes tedious) to derive. We present them here briefly to make the paper self contained.

A. Coulomb wave function

For the Coulomb wave functions we followed Gaspard and Sparenberg [51]. In that paper, the analytical properties are emphazised. This is relevant to us because we call the Coulomb wave functions at real and purely imaginary arguments. We employed MATHEMATICA and SCIPY special functions in PYTHON for our numerical implementation. We checked for a number of arguments that our implementation agrees with the precise numerical routines by Michel [82].

The regular Coulomb wave function is

$$F_l(\eta,\rho) = C_l(\eta)\rho^{l+1}e^{i\rho}M(l+1+i\eta,2l+2,-i2\rho). \tag{44}$$

Here, $\eta = k_c/k$ is the Sommerfeld parameter, and $\rho = kr$. For bound states with energy $E = -\hbar^2\gamma^2/(2m)$ we have $k = -i\gamma$, and the arguments $\eta = -ik_c/\gamma$, and $\rho = i2\gamma r$ are purely imaginary. In Eq. (44), we employed Kummer's function $M(a,b,z)$, or the confluent hypergeometric function ${}_1F_1(a,b,z) = M(a,b,z)$. The η-dependent normalization $C_l(\eta)$, not to be confused with the ANC and distinct from it by its argument, is

$$C_l(\eta) = \frac{(2\eta)^l}{(2l+1)!}\sqrt{\frac{2\pi\eta w_l(\eta)}{e^{2\pi\eta}-1}}, \tag{45}$$

with

$$w_l(\eta) = \prod_{j=0}^{l}\left(1+\frac{j^2}{\eta^2}\right). \tag{46}$$

The incoming and outgoing Coulomb wave functions are

$$H_l^{\pm}(\eta,\rho) = D_l^{\pm}(\eta)\rho^{l+1}e^{\pm i\rho}U(l+1\pm i\eta,2l+2,\mp i2\rho). \tag{47}$$

Here, U denotes Tricomi's function (or the confluent hypergeometric function of the second kind) and the normalization is

$$D_l^{\pm}(\eta) = \mp i2(-1)^l e^{\pi\eta}\frac{(2l+1)!C_l(\eta)}{\Gamma(l+1\mp i\eta)}. \tag{48}$$

The irregular Coulomb wave function is then defined as

$$G_l(\eta,\rho) = \frac{1}{2}\left[H_l^+(\eta,\rho) + H_l^-(\eta,\rho)\right]. \tag{49}$$

We are interested in low-energy phenomena and therefor seek approximations for Coulomb wave functions for $\eta \gg 1$. Following [50, Chapter 33.9] we expand the Coulomb wave functions into a series of modified Bessel functions whose coefficients decrease with inverse powers of η. Thus, ($\eta \equiv k_c/k$ and $\rho \equiv kR$)

$$\begin{aligned} F_0(\eta,\rho) &= \frac{C_0(\eta)}{2\eta}\sum_{n=1}^{\infty} b_n(2k_cR)^{\frac{n}{2}}I_n(2\sqrt{2k_cR}), \\ G_0(\eta,\rho) &= \frac{2}{\beta_0(\eta)C_0(\eta)}\sum_{n=1}^{\infty}(-1)^n b_n(2k_cR)^{\frac{n}{2}}K_n(2\sqrt{2k_cR}) \end{aligned} \tag{50}$$

.

Here,

$$\begin{aligned} b_1 &= 1, \\ b_2 &= 0, \\ b_3 &= -\frac{1}{4\eta^2}, \\ b_4 &= -\frac{1}{12\eta^2}, \end{aligned} \tag{51}$$

and all other b_n are of order $\mathcal{O}(\eta^{-4})$ or smaller. We have

$$\beta_0(\eta) = -1 + \mathcal{O}(\eta^{-4}). \tag{52}$$

Similar expressions exist for nonzero orbital angular momentum.

We also need to know similar approximations for the Coulomb wave functions for purely imaginary momentum $k = i\gamma$. In the weak-binding limit $\gamma \to 0$, the regular Coulomb wave function becomes [50, Eq. 13.8.12]

$$F_l\left(\frac{k_c}{i\gamma}, i\gamma r\right) \approx (i\gamma r)^{l+1} C_l(-ik_c/\gamma) \frac{(2l+1)!}{(2k_c r)^{l+1/2}} I_{2l+1}(2\sqrt{2k_c r}). \tag{53}$$

The Coulomb wave functions G_l and H_l^+ are based on Tricomi's function. For $\gamma \to 0$ we use (see Ref. [83])

$$\lim_{a\to\infty} U(a, b, z/a)\Gamma(1 + a - b) = 2z^{\frac{1-b}{2}} K_{b-1}(2\sqrt{z}). \tag{54}$$

We see that Coulomb wave functions are approximated by modified Bessel functions as the momentum goes to zero. Let us also consider approximations of the latter. We have

$$\begin{aligned} I_n(z) &\approx \left(\frac{z}{2}\right)^n \left(\frac{1}{n!} + \frac{z^2}{4(n+1)!}\right), \\ K_n(z) &\approx \frac{1}{2}\left(\frac{2}{z}\right)^n \left((n-1)! + \frac{(n-2)!z^2}{4}\right), \end{aligned} \tag{55}$$

valid for $z \ll 1$, see [50, Chapters 10.25 and 10.31]. We also have

$$\begin{aligned} I_n(z) &\approx \frac{e^z}{\sqrt{2\pi z}}\left(1 - \frac{a_1(n)}{z}\right), \\ K_n(z) &\approx \sqrt{\frac{\pi}{2z}} e^{-z}\left(1 + \frac{a_1(n)}{z}\right), \end{aligned} \tag{56}$$

valid for $z \to \infty$, see [50, Chapter 10.40]. Here,

$$a_1(n) \equiv \frac{4n^2 - 1}{8}. \tag{57}$$

B. Estimate for the asymptotic normalization coefficient and inter-ion distance

We want to compute an estimate for the ANC. For the δ-shell potential, the bound-state wave function can be written as follows.

$$u_l(r) = \begin{cases} C_l \frac{W_{-\frac{k_c}{\gamma}, l+\frac{1}{2}}(2\gamma R)}{F_l\left(\frac{k_c}{i\gamma}, i\gamma R\right)} F_l\left(\frac{k_c}{i\gamma}, i\gamma r\right) & \text{, for } r < R, \\ C_l W_{-\frac{k_c}{\gamma}, l+\frac{1}{2}}(2\gamma r) & \text{, for } r > R. \end{cases}$$

Here, we employed the Whittaker function W (which is proportional to the outgoing Coulomb wave function for bound states [50]), and C_l is the ANC by definition. We have

$$W_{\kappa,\mu}(z) = e^{-\frac{z}{2}} z^{\mu+\frac{1}{2}} U(1/2 + \mu - \kappa, 1 + 2\mu, z) \tag{58}$$

The ANC is determined by the normalization condition

$$\begin{aligned} 1 &= \int_0^\infty dr\, |u_l(r)|^2 \\ &= C_l^2 \int_R^\infty dr \left(W_{-\frac{k_c}{\gamma}, l+\frac{1}{2}}(2\gamma r)\right)^2 \\ &\quad + \left| C_l \frac{W_{-\frac{k_c}{\gamma}, l+\frac{1}{2}}(2\gamma R)}{F_l\left(\frac{k_c}{i\gamma}, i\gamma R\right)} \right|^2 \int_0^R dr \left| F_l\left(\frac{k_c}{i\gamma}, i\gamma r\right)\right|^2 \end{aligned} \tag{59}$$

To perform the integration, we need to make approximations. As we are interested in the case of weak binding, i.e. $\gamma \to 0$, we use the approximation (54). Thus,

$$W_{-\frac{k_c}{\gamma}, l+\frac{1}{2}}(2\gamma r) \approx \frac{2(2k_c r)^{-l-\frac{1}{2}}}{\Gamma(k_c/\gamma - l)} K_{2l+1}\left(2\sqrt{2k_c r}\right). \tag{60}$$

Here, we approximated $e^{-\gamma r} \approx 1$. We note that the bound-state momentum enters as the argument of the Γ function. To simplify matters further, we approximate

$$\Gamma(k_c/\gamma - l)\left(\frac{k_c}{\gamma}\right)^{l+1} \approx \Gamma(k_c/\gamma + 1), \tag{61}$$

which is correct in leading order when $\gamma \ll k_c$. Then

$$W_{-\frac{k_c}{\gamma}, l+\frac{1}{2}}(2\gamma r) \approx \frac{2\sqrt{2k_c r}}{\Gamma(1 + k_c/\gamma)} K_{2l+1}\left(2\sqrt{2k_c r}\right). \tag{62}$$

In the weak-binding limit $\gamma \to 0$, we use the approximation (53) for the regular Coulomb wave function. The integral (59) can now be evaluated exactly (e.g. via MATHEMATICA), but we did not find the result particularly illuminating. However, for $l = 0$ one can then take the limit $R \to 0$ and finds

$$C_0 \approx \sqrt{6k_c}\Gamma(1 + k_c/\gamma). \tag{63}$$

This is the result from leading-order Coulomb halo EFT [65].

For further analytical insights we return to Eqs. (62) and (53), and assume $k_c R \gg 1$. This allows us to use the leading terms of Eqs. (50). We change the integration variable to $z = \sqrt{2k_c r}$ and perform the integration (59). Keeping only the leading term in $k_c R \gg 1$ yields

$$C_l \approx \frac{\Gamma(1 + k_c/\gamma)}{\sqrt{\pi R}} e^{2\sqrt{2k_c R}}. \tag{64}$$

Replacing $R \to D$ yields the result presented in Table I.

Similar computations allow us also to give an estimate for the squared inter-ion distance (19). Making the same approximations as in the computation of the ANC we find (for orbital angular momentum $l = 0$)

$$\langle r^2 \rangle \approx \begin{cases} \frac{9}{35} k_c^{-2}, & \text{for } R \to 0, \\ R^2, & \text{for } k_c R \gg 1. \end{cases} \tag{65}$$

The results are strikingly different from each other because the wave function is strongly localized and peaked around $r = R$ in for large Coulomb momenta. We see in particular that the inter-ion distance does not depend on the bound-state momentum, and this is in stark contrast to the case without Coulomb, where $\langle r^2 \rangle \propto \gamma^{-2}$. Replacing $R \to D$ yields the expressions presented in Table I.

C. Estimate for the resonance width

For the δ-shell potential, the resonance width is given in Eq. (29).

Using the approximation (50) the inverse width becomes in leading order of $k_c/\kappa \gg 1$

$$\frac{E}{\Gamma} \approx \frac{\kappa R}{3C_0^2(\eta)} \frac{\sqrt{2k_c R}(I_1 K_4 - I_4 K_1) - 3(I_1 K_3 + I_3 K_1)}{I_1^2} \tag{66}$$

.

Here, we have suppressed the arguments of the modified Bessel function, i.e. $I_n \equiv I_n(2\sqrt{2k_c R})$ and $K_n \equiv K_n(2\sqrt{2k_c R})$.

We consider two cases. For zero-range interactions, we take $R \to 0$ and obtain

$$\left.\frac{\Gamma}{E}\right|_{R\to 0} \approx 24\pi \frac{k_c^2}{\kappa^2} e^{-2\pi \frac{k_c}{\kappa}}. \tag{67}$$

Here, we used the expansions (55). The physically relevant case $k_c R \gg 1$ is more interesting. We use the expansions (56) and find

$$\left.\frac{\Gamma}{E}\right|_{k_c R \gg 1} \approx 4 \frac{k_c}{\kappa^2 R} e^{4\sqrt{2k_c R}} e^{-2\pi \frac{k_c}{\kappa}}. \tag{68}$$

Replacing $R \to D$ yields the results presented in Subsection II A.

D. Estimates for effective-range parameters

We start from the effective-range parameters given in Eq. (24). These expressions contain the strength λ_0 of the δ-shell potential. For a resonance with energy $E = \hbar^2\kappa^2/(2m)$ this parameter fulfills Eq. (26). We assume $\kappa \ll k_c$ and use the approximation (50), focusing on orbital angular momentum $l = 0$. This yields

$$(\lambda_0 R)^{-1} \approx -2 I_1 K_1 - \frac{\kappa^2 R}{8 k_c \sqrt{2k_c R}}, \tag{69}$$

and we have omitted higher-order corrections in κ/k_c. Here, and in what follows the modified Bessel functions have arguments $I_n \equiv I_n(2\sqrt{2k_c R})$ and similar for K_n.

We insert the expression (69) into the Eq. (24) for the s-wave scattering length and find

$$a_0^{-1} = -\frac{\kappa^2 R}{4 I_1^2 \sqrt{2k_c R}}. \tag{70}$$

Again, we consider two approximations. For $2\sqrt{2k_c R} \gg 1$, we take the leading approximation of Eqs. (56) and find

$$a_0 = -(\pi \kappa^2 R)^{-1} e^{4\sqrt{2k c_D}}. \tag{71}$$

For $R \to 0$, we take the approximations (55) and find $a_0 = -6k_c/\kappa^2$. Replacing $R \to D$ yields the expressions given in Table I.

We turn to the effective range of Eq. (24) and employ the leading term $(\lambda_0 R)^{-1} \approx -2 I_1 K_1$ from Eq. (69). This yields

$$r_0 = \frac{1}{3k_c} \left(1 + \frac{2(2kcR)^{3/2} I_2 K_1 - k_c R}{I_1^2} \right). \tag{72}$$

Again, we consider two approximations. For $2\sqrt{2k_c R} \gg 1$, we take the Eqs. (56) and find [8]

$$r_0 = (3k_c)^{-1} - \pi R\, e^{-4\sqrt{2k_c R}}. \tag{73}$$

For $R \to 0$, we employ the approximations (55) and find $r_0 = \mathcal{O}(R)$). Replacing $R \to D$ yields the expressions given in Table I and in Eq. (6).

E. Derivatives of Coulomb wave functions

We limit the discussion to orbital angular momentum $l = 0$ and positive energies. For $k \ll k_c$ we find ($z \equiv 2\sqrt{2k_c r}$) from Eq. (50) that

$$\begin{aligned} F_0(k_c/k, kr) &\propto z I_1(z), \\ G_0(k_c/k, kr) &\propto z K_1(z). \end{aligned} \tag{74}$$

Here, we neglected any constants and functions that depend on k and k_c, but not on r. We see that only the combination $2k_c r$ enters, and it is clear that a derivative with respect to r will yield a factor k_c rather than k. Taking a derivative becomes particularly simple for strong Coulomb interactions as $k_c r \gg 1$ practically holds for all distances exceeding 1 fm or so. We use the approximations (56) and find

$$\begin{aligned} F_0(k_c/k, kr) &\propto \sqrt{\frac{z}{2\pi}} e^z, \\ G_0(k_c/k, kr) &\propto \sqrt{\frac{\pi z}{2}} e^{-z}. \end{aligned} \tag{75}$$

Taking the derivative with respect to r, and using $z \gg 1$ yields

$$\begin{aligned} \frac{d}{dr} F_0(k_c/k, kr) &\approx +4k_c F_0(k_c/k, kr), \\ \frac{d}{dr} G_0(k_c/k, kr) &\approx -4k_c G_0(k_c/k, kr). \end{aligned} \tag{76}$$

F. Square well plus Coulomb

The potential is

$$V(r) = \begin{cases} -\frac{\hbar^2 q^2}{2m}, & r < R \\ \frac{Z_1 Z_2 \alpha \hbar}{r} & r > R. \end{cases} \tag{77}$$

We limit ourselves to s waves. Solutions with positive energy $E = \hbar^2 k^2/(2m)$ are

$$u(r) = \begin{cases} \frac{\cos\delta F_0\left(\frac{k_c}{k}, kR\right) + \sin\delta G_0\left(\frac{k_c}{k}, kR\right)}{\sin p_k R} \sin p_k r, & r < R \\ \cos\delta F_0\left(\frac{k_c}{k}, kr\right) + \sin\delta G_0\left(\frac{k_c}{k}, kr\right), & r > R. \end{cases} \tag{78}$$

Here, $p_k \equiv \sqrt{k^2 + q^2}$. The phase shifts fulfill

$$\cot\delta = \frac{G_0'\left(\frac{k_c}{k}, kR\right)\sin p_k R - \frac{p}{k} G_0\left(\frac{k_c}{k}, kR\right)\cos p_k R}{F_0'\left(\frac{k_c}{k}, kR\right)\sin p_k R - \frac{p_k}{k} F_0\left(\frac{k_c}{k}, kR\right)\cos p_k R} \tag{79}$$

Here, we used $F_0'(\eta, z) \equiv \frac{d}{dz} F_0(\eta, z)$ and similar for the irregular Coulomb wave function. A resonance at energy $E_\kappa \equiv \hbar^2\kappa^2/(2m)$ fulfills

$$p_\kappa \cot p_\kappa R = \kappa \frac{G_0'\left(\frac{k_c}{\kappa}, \kappa R\right)}{G_0\left(\frac{k_c}{\kappa}, \kappa R\right)} \tag{80}$$

The resonance width Γ fulfills

$$\frac{E_\kappa}{\Gamma} = \frac{G_0}{4}\left(\frac{q^2}{p_\kappa^2} G_0' + \kappa \dot{G}_0' - \kappa \frac{G_0' \dot{G}_0}{G_0} + \frac{\kappa R G_0}{\sin^2 p_\kappa R}\right) . \tag{81}$$

Here, we used $\dot{G}_0(kc/\kappa, \kappa R) \equiv \frac{d}{d\kappa} G_0(k_c/\kappa, \kappa R)$, and we dropped the arguments for all Coulomb wave function. For a given resonance energy and width, one can solve Eqs. (80) and (81) for the parameters (q, R) of the potential. Once these are known, the phase shifts result from Eq. (79). As the square well can hold an arbitrary number of bound states, the solutions are not unique. However, low-energy data such as the $\alpha - \alpha$ phase shifts exhibit sensitivity to such details only at energies above about 1.7 MeV.

[1] E. G. Adelberger, A. García, R. G. Hamish Robertson, K. A. Snover, A. B. Balantekin, K. Heeger, M. J. Ramsey-Musolf, D. Bemmerer, A. Junghans, C. A. Bertulani, J.-W. Chen, H. Costantini, P. Prati, M. Couder, E. Uberseder, M. Wiescher, R. Cyburt, B. Davids, S. J. Freedman, M. Gai, D. Gazit, L. Gialanella, G. Imbriani, U. Greife, M. Hass, W. C. Haxton, T. Itahashi, K. Kubodera, K. Langanke, D. Leitner, M. Leitner, P. Vetter, L. Winslow, L. E. Marcucci, T. Motobayashi, A. Mukhamedzhanov, R. E. Tribble, Kenneth M. Nollett, F. M. Nunes, T.-S. Park, P. D. Parker, R. Schiavilla, E. C. Simpson, C. Spitaleri, F. Strieder, H.-P. Trautvetter, K. Suemmerer, and S. Typel, "Solar fusion cross sections. ii. the *pp* chain and cno cycles," Rev. Mod. Phys. **83**, 195–245 (2011).

[2] B. Buck, C. B. Dover, and J. P. Vary, "Simple potential model for cluster states in light nuclei," Phys. Rev. C **11**, 1803–1821 (1975).

[3] A. V. Kulik and V. D. Mur, "dt, d^3he, and $p\alpha$ scattering in the vicinity of the 5he* and 5li* resonances," Phys. Atom. Nuclei **66**, 87 (2003).

[4] S. Typel and G. Baur, "Electromagnetic strength of neutron and proton single-particle halo nuclei," Nuclear Physics A **759**, 247 – 308 (2005).

[5] A. Grassi, G. Mangano, L. E. Marcucci, and O. Pisanti, "$\alpha + d \to^6$ Li $+ \gamma$ astrophysical s factor and its implications for big bang nucleosynthesis," Phys. Rev. C **96**, 045807 (2017).

[6] J. Hamilton, I. Øverbö, and B. Tromborg, "Coulomb corrections in non-relativistic scattering," Nuclear Physics B **60**, 443 – 477 (1973).

[7] V. D. Mur and V. S. Popov, "Coulomb problem with short-range interaction: Exactly solvable model," Theoretical and Mathematical Physics **65**, 1132–1140 (1985).

[8] V. D. Mur, B. M. Karnakov, S. G. Pozdnyakov, and V. S. Popov, "Low-energy parameters of the dt and d^{3}He systems," Physics of Atomic Nuclei **56**, 217–226 (1993).

[9] Jean-Marc Sparenberg, Pierre Capel, and Daniel Baye, "Influence of low-energy scattering on loosely bound states," Phys. Rev. C **81**, 011601 (2010).

[10] R. Yarmukhamedov and D. Baye, "Connection between effective-range expansion and nuclear vertex constant or asymptotic normalization coefficient," Phys. Rev. C **84**, 024603 (2011).

[11] O. L. Ramírez Suárez and J.-M. Sparenberg, "Phase-shift parametrization and extraction of asymptotic normalization constants from elastic-scattering data," Phys. Rev. C **96**, 034601 (2017).

[12] L. D. Blokhintsev, A. S. Kadyrov, A. M. Mukhamedzhanov, and D. A. Savin, "Extrapolation of scattering data to the negative-energy region. iii. application to the $p -^{16}$ O system," Phys. Rev. C **98**, 064610 (2018).

[13] R. Higa, H.-W. Hammer, and U. van Kolck, "$\alpha\alpha$ scattering in halo effective field theory," Nuclear Physics A **809**, 171 – 188 (2008).

[14] Emil Ryberg, Christian Forssén, H.-W. Hammer, and Lucas Platter, "Effective field theory for proton halo nuclei," Phys. Rev. C **89**, 014325 (2014).

[15] Shi-Sheng Zhang, M. S. Smith, Zhong-Shu Kang, and Jie Zhao, "Microscopic self-consistent study of neon halos with resonant contributions," Phys. Lett. B **730**, 30 – 35 (2014).

[16] Renato Higa, Gautam Rupak, and Akshay Vaghani, "Radiative 3he(α,γ)7be reaction in halo effective field theory," The European Physical Journal A **54**, 89 (2018).

[17] P. Capel, D. R. Phillips, and H.-W. Hammer, "Dissecting reaction calculations using halo effective field theory and

ab initio input," Phys. Rev. C **98**, 034610 (2018).
[18] Xilin Zhang, Kenneth M. Nollett, and Daniel R. Phillips, "S-factor and scattering parameters from ^{3}He + ^{4}He $\to$ ^{7}Be + γ data," arXiv e-prints , arXiv:1811.07611 (2018), arXiv:1811.07611 [nucl-th].
[19] Thomas Neff, "Microscopic calculation of the ^{3}He$(\alpha,\gamma)^7$Be and ^{3}**H**$(\alpha,\gamma)^7$Li capture cross sections using realistic interactions," Phys. Rev. Lett. **106**, 042502 (2011).
[20] K. M. Nollett, R. B. Wiringa, and R. Schiavilla, "Six-body calculation of the α-deuteron radiative capture cross section," Phys. Rev. C **63**, 024003 (2001).
[21] Sofia Quaglioni and Petr Navrátil, "*Ab Initio* many-body calculations of $n-^3$H, $n-^4$He, $p-^{3,4}$He, and $n-^{10}$Be scattering," Phys. Rev. Lett. **101**, 092501 (2008).
[22] Guillaume Hupin, Sofia Quaglioni, and Petr Navrátil, "Unified description of ^{6}Li structure and deuterium-^{4}He dynamics with chiral two- and three-nucleon forces," Phys. Rev. Lett. **114**, 212502 (2015).
[23] Jérémy Dohet-Eraly, Petr Navrátil, Sofia Quaglioni, Wataru Horiuchi, Guillaume Hupin, and Francesco Raimondi, "He3(α,γ)be7 and h3(α,γ)li7 astrophysical s factors from the no-core shell model with continuum," Physics Letters B **757**, 430 – 436 (2016).
[24] Sergey Dubovichenko and Albert Dzhazairov-Kakhramanov, "Study of the nucleon radiative captures 8li(n,γ)9li, 9be(p,γ)10b, 10be(n,γ)11be, 10b(p,γ)11c, and 16o(p,γ)17f at thermal and astrophysical energies," International Journal of Modern Physics E **26**, 1630009 (2017).
[25] Pierre Descouvemont, Abderrahim Adahchour, Carmen Angulo, Alain Coc, and Elisabeth Vangioni-Flam, "Compilation and r-matrix analysis of big bang nuclear reaction rates," Atomic Data and Nuclear Data Tables **88**, 203 – 236 (2004).
[26] J. T. Huang, C. A. Bertulani, and V. Guimarães, "Radiative capture of nucleons at astrophysical energies with single-particle states," Atomic Data and Nuclear Data Tables **96**, 824 – 847 (2010).
[27] J. Dobaczewski, W. Nazarewicz, and P.-G. Reinhard, "Error estimates of theoretical models: a guide," Journal of Physics G: Nuclear and Particle Physics **41**, 074001 (2014).
[28] R. J. Furnstahl, D. R. Phillips, and S. Wesolowski, "A recipe for eft uncertainty quantification in nuclear physics," Journal of Physics G: Nuclear and Particle Physics **42**, 034028 (2015).
[29] M. R. Schindler and D. R. Phillips, "Bayesian methods for parameter estimation in effective field theories," Ann. Phys. **324**, 682 – 708 (2009).
[30] R. J. Furnstahl, G. Hagen, T. Papenbrock, and K. A. Wendt, "Infrared extrapolations for atomic nuclei," Journal of Physics G: Nuclear and Particle Physics **42**, 034032 (2015).
[31] E. A. Coello Pérez and T. Papenbrock, "Effective field theory for nuclear vibrations with quantified uncertainties," Phys. Rev. C **92**, 064309 (2015).
[32] B. D. Carlsson, A. Ekström, C. Forssén, D. Fahlin Strömberg, G. R. Jansen, O. Lilja, M. Lindby, B. A. Mattsson, and K. A. Wendt, "Uncertainty analysis and order-by-order optimization of chiral nuclear interactions," Phys. Rev. X **6**, 011019 (2016).
[33] A. M. Mukhamedzhanov and R. E. Tribble, "Connection between asymptotic normalization coefficients, subthreshold bound states, and resonances," Phys. Rev. C **59**, 3418–3424 (1999).
[34] L. Blokhintsev, I. Borbely, and E. I. Dolinskii, "Nuclear vertex constants," Sov. J. Part. Nucl. (Engl. Transl.); (United States) **8**, 485 (1977).
[35] A. M. Mukhamedzhanov and N. K. Timofeyuk, "Astrophysical S-factor for the reaction ^{7}Be+p $\to$ ^{8}B+γ." Soviet Journal of Experimental and Theoretical Physics Letters **51**, 282–284 (1990).
[36] P. F. Bedaque and U. van Kolck, "Effective field theory for few-nucleon systems," Annual Review of Nuclear and Particle Science **52**, 339–396 (2002), nucl-th/0203055.
[37] C. A. Bertulani, H.-W. Hammer, and U. van Kolck, "Effective field theory for halo nuclei: shallow p-wave states," Nucl. Phys. A **712**, 37 – 58 (2002).
[38] H.-W. Hammer, C. Ji, and D. R. Phillips, "Effective field theory description of halo nuclei," Journal of Physics G: Nuclear and Particle Physics **44**, 103002 (2017).
[39] T. Papenbrock, Talk at the workshop *Progress in Ab Initio Techniques in Nuclear Physics*, TRIUMF, Vancouver, B.C. (February 2019).
[40] C. H. Schmickler, H. W. Hammer, and A. G. Volosniev, "Universal physics of bound states of a few charged particles," arXiv e-prints , arXiv:1904.00913 (2019), arXiv:1904.00913 [nucl-th].
[41] A. I. Baz', I. A. B. Zeldovich, and A. M. Perelomov, *Scattering, reactions and decay in nonrelativistic quantum mechanics: (Rasseyanie, reaktsii i raspady v nerelyativistskoi kvantovoi mekhanike)*, NASA Technical Translation (Israel Program for Scientific Translations, 1969).
[42] S. Elhatisari and D. Lee, "Causality bounds for neutron-proton scattering," The European Physical Journal A **48**, 110 (2012).
[43] Sebastian König, Dean Lee, and H.-W. Hammer, "Causality constraints for charged particles," Journal of Physics G: Nuclear and Particle Physics **40**, 045106 (2013).
[44] B. Buck and A. A. Pilt, "Alpha-particle and triton cluster states in 19f," Nuclear Physics A **280**, 133 – 160 (1977).
[45] E. Ryberg, C. Forssén, D. R. Phillips, and U. van Kolck, "Finite-size effects in heavy halo nuclei from effective field theory," arXiv e-prints , arXiv:1905.01107 (2019), arXiv:1905.01107 [nucl-th].
[46] C. A. Gagliardi, R. E. Tribble, A. Azhari, H. L. Clark, Y.-W. Lui, A. M. Mukhamedzhanov, A. Sattarov, L. Trache, V. Burjan, J. Cejpek, V. Kroha, Š. Piskoř, and J. Vincour, "Tests of transfer reaction determinations of astrophysical s factors," Phys. Rev. C **59**, 1149–1153 (1999).
[47] S. V. Artemov, S. B. Igamov, K. I. Tursunmakhatov, and R. Yarmukhamedov, "Determination of nuclear vertex constants (asymptotic normalization coefficients) for the virtual decays 3he $\to$ d + p and 17f $\to$ 16o + p and their use for extrapolating astrophysical s-factors of the radiative proton capture by the deuteron and the 16o nucleus at very low energies," Bulletin of the Russian Academy of Sciences: Physics **73**, 165–170 (2009).
[48] G. Breit and W. G. Bouricius, "A boundary value condition for proton-proton scattering," Phys. Rev. **74**, 1546–1547 (1948).
[49] L. P. Kok, J. W. de Maag, H. H. Brouwer, and H. van Haeringen, "Formulas for the δ-shell-plus-coulomb potential for all partial waves," Phys. Rev. C **26**, 2381–2396 (1982).

[50] DLMF, "NIST Digital Library of Mathematical Functions," http://dlmf.nist.gov/, Release 1.0.23 of 2019-06-15, F. W. J. Olver, A. B. Olde Daalhuis, D. W. Lozier, B. I. Schneider, R. F. Boisvert, C. W. Clark, B. R. Miller and B. V. Saunders, eds.

[51] David Gaspard and Jean-Marc Sparenberg, "Effective-range function methods for charged particle collisions," Phys. Rev. C **97**, 044003 (2018).

[52] Eugene P. Wigner, "Lower limit for the energy derivative of the scattering phase shift," Phys. Rev. **98**, 145–147 (1955).

[53] H. Friedrich, *Scattering Theory* (Springer Berlin Heidelberg, 2015).

[54] R. F. Garcia Ruiz et. al, *Towards laser spectroscopy of exotic fluorine isotopes*, Proposal INTC-I-171 CERN-INTC-2016-037 (CERN, 2016).

[55] Alejandro Sonzogni, *NuDat2.7*, Tech. Rep. (National Nuclear Data Center (NNDC), Brookhaven National Laboratory, 2019).

[56] N. P. Heydenburg and G. M. Temmer, "Alpha-alpha scattering at low energies," Phys. Rev. **104**, 123–134 (1956).

[57] S. A. Afzal, A. A. Z. Ahmad, and S. Ali, "Systematic survey of the $\alpha - \alpha$ interaction," Rev. Mod. Phys. **41**, 247–273 (1969).

[58] G. Rasche, "Effective range analysis of s- and d-wave $\alpha-\alpha$ scattering," Nuclear Physics A **94**, 301 – 312 (1967).

[59] R. Kamouni and D. Baye, "Scattering length and effective range for collisions between light ions within a microscopic model," Nuclear Physics A **791**, 68 – 83 (2007).

[60] S. Elhatisari, D. Lee, G. Rupak, E. Epelbaum, H. Krebs, T. A. Lähde, T. Luu, and U.-G. Meißner, "Ab initio alpha–alpha scattering," Nature **528**, 111–114 (2015).

[61] R. Morlock, R. Kunz, A. Mayer, M. Jaeger, A. Müller, J. W. Hammer, P. Mohr, H. Oberhummer, G. Staudt, and V. Kölle, "Halo properties of the first $1/2^+$ state in ^{17}f from the $^{16}o(p,\gamma)^{17}f$ reaction," Phys. Rev. Lett. **79**, 3837–3840 (1997).

[62] Sergey Dubovichenko, Nassurlla Burtebayev, Albert Dzhazairov-Kakhramanov, Denis Zazulin, Zhambul Kerimkulov, Marzhan Nassurlla, Chingis Omarov, Alesya Tkachenko, Tatyana Shmygaleva, Stanislaw Kliczewski, and Turlan Sadykov, "New measurements and phase shift analysis of p 16o elastic scattering at astrophysical energies," Chinese Physics C **41**, 014001 (2017).

[63] R. A. Blue and W. Haeberli, "Polarization of protons elastically scattered by oxygen," Phys. Rev. **137**, B284–B293 (1965).

[64] Walter Trächslin and Louis Brown, "Polarization and phase shifts in 12c(p,p)12c and 16o(p,p)16o from 1.5 to 3 mev," Nuclear Physics A **101**, 273 – 287 (1967).

[65] Emil Ryberg, Christian Forssén, H.-W. Hammer, and Lucas Platter, "Range corrections in proton halo nuclei," Annals of Physics **367**, 13 – 32 (2016).

[66] I. Angeli and K.P. Marinova, "Table of experimental nuclear ground state charge radii: An update," At. Data Nucl. Data Tables **99**, 69 – 95 (2013).

[67] G. Hagen, T. Papenbrock, and M. Hjorth-Jensen, "*Ab Initio* Computation of the ^{17}**F** Proton Halo State and Resonances in $A = 17$ Nuclei," Phys. Rev. Lett. **104**, 182501 (2010).

[68] N. J. Stone, *Table of Nuclear Magnetic Dipole and Electric Quadrupole Moments*, Tech. Rep. INDC(NDS)–0658 (International Atomic Energy Agency (IAEA), 2014).

[69] Emil Ryberg, Christian Forssén, H.-W. Hammer, and Lucas Platter, "Constraining low-energy proton capture on beryllium-7 through charge radius measurements," The European Physical Journal A **50**, 170 (2014).

[70] L. G. Keller and W. Haeberli, "Vector-polarization measurements and phase-shift analysis for $d - \alpha$ scattering between 3 and 11 mev," Nuclear Physics A **156**, 465 – 476 (1970).

[71] W. Grüebler, P. A. Schmelzbach, V. König, R. Risler, and D. Boerma, "Phase-shift analysis of $d - \alpha$ elastic scattering between 3 and 17 mev," Nuclear Physics A **242**, 265 – 284 (1975).

[72] V. M. Krasnopol'sky, V. I. Kukulin, E. V. Kuznetsova, J. Horáek, and N. M. Queen, "Energy-dependent phase-shift analysis of ^{2}H+^{4}he scattering in the energy range $0.87 < e_d < 5.24$ mev," Phys. Rev. C **43**, 822–834 (1991).

[73] A. M. Mukhamedzhanov, L. D. Blokhintsev, and B. F. Irgaziev, "Reexamination of the astrophysical s factor for the α+$d \to {}^6$li+γ reaction," Phys. Rev. C **83**, 055805 (2011).

[74] L. D. Blokhintsev and D. A. Savin, "Analytic continuation of the effective-range expansion as a method for determining the features of bound states: Application to the 6li nucleus," Physics of Atomic Nuclei **77**, 351–361 (2014).

[75] L. D. Blokhintsev, V. I. Kukulin, A. A. Sakharuk, D. A. Savin, and E. V. Kuznetsova, "Determination of the $^6\alpha$+d vertex constant (asymptotic coefficient) from the ^{4}He+d phase-shift analysis," Phys. Rev. C **48**, 2390–2394 (1993).

[76] L. D. Blokhintsev, S. B. Igamov, M. M. Nishonov, and R. Yarmukhamedov, "Calculation of the nuclear vertex constant (asymptotic normalization coefficient) for the virtual decay 6li $\to \alpha$ + d on the basis of the three-body model and application of the result in describing the astrophysical nuclear reaction d(α, γ)6li at ultralow energies," Physics of Atomic Nuclei **69**, 433–444 (2006).

[77] E. M. Tursunov, S. A. Turakulov, and P. Descouvemont, "Theoretical analysis of the astrophysical s-factor for the capture reaction α+$d \to^6$ Li+γ in the two-body model," Physics of Atomic Nuclei **78**, 193–200 (2015).

[78] R. J. Spiger and T. A. Tombrello, "Scattering of he^3 by he^4 and of he^4 by tritium," Phys. Rev. **163**, 964–984 (1967).

[79] W. R. Boykin, S. D. Baker, and D. M. Hardy, "Scattering of 3he and 4he from polarized 3he between 4 and 10 mev," Nuclear Physics A **195**, 241 – 249 (1972).

[80] Q. I. Tursunmahatov and R. Yarmukhamedov, "Determination of the ^{3}he $+\alpha \to^7$be asymptotic normalization coefficients, the nuclear vertex constants, and their application for the extrapolation of the ^{3}he$(\alpha,\gamma)^7$be astrophysical s factors to the solar energy region," Phys. Rev. C **85**, 045807 (2012).

[81] S. B. Igamov and R. Yarmukhamedov, "Modified two-body potential approach to the peripheral direct capture astrophysical $a + a \to b + \gamma$ reaction and asymptotic normalization coefficients," Nuclear Physics A **781**, 247 – 276 (2007).

[82] N. Michel, "Precise coulomb wave functions for a wide range of complex l, η, and z," Computer Physics Communications **176**, 232 – 249 (2007).

[83] Milton Abramowitz and Irene A. Stegun, *Handbook of Mathematical Functions with Formulas, Graphs, and Mathematical Tables* (Dover, New York City, 1964).